

UNIVERSITY OF CAPE TOWN

Department of Mechanical Engineering

RONDEBOSCH, CAPE TOWN
SOUTH AFRICA



MEC4110W - 2017

PROJECT No:

29-C

***Chemical Smoothing of 3D Printed
ABS***

Andrea Pearce

SUPERVISOR:

Dr Reuben Govender

I. Abstract

This report investigates the characterization of 3D printed materials in order to improve design guidelines and material properties of this relatively new manufacturing method – focussing on the requirements of surface finish and strength. The effects of chemical exposure to parts produced through Fused Deposition Modelling is therefore examined, regarding the ability of treatments to improve the surface finish of parts as well as their effect on the tensile properties of parts.

Parts were additively manufactured through the process of FDM using the filament material acrylonitrile-butadiene-styrene (ABS). Parts were printed both flat and upright so that in-plane as well as interlaminar tensile properties could be investigated. Chemical treatment methods included dipping in an acetone solution and acetone vapour smoothing. Microscopic images as well as surface roughness tests examined the effect of these smoothing methods on the surface finish of each specimen and average roughness values were compared before and after smoothing. Lastly, the tensile properties of each specimen were investigated through elongation until fracture within a Zwick tensile tester. Strain readings were obtained from an extensometer as well as Digital Image Correlation and these differing results were compared. The strength data of treated and untreated specimens, in both testing directions were also compared.

Results obtained from the investigation showed that dipping was a more effective smoothing method than cold vapour smoothing, although parts were adequately smoothed using both techniques. It was also found that in-plane specimens could withstand higher stress values than interlaminar specimens – 28MPa compared with 18.8MPa, and were more ductile as they withstood greater elongation before fracturing. There was, however, no significant difference between strength data of treated and untreated specimens – for both smoothing methods. ABS parts can therefore be smoothed to improve their surface finish without altering their strength properties to a large degree.

II. Acknowledgements

I would like to thank my supervisor, Dr. Reuben Govender, for the guidance and support that he has given me throughout this project as well as giving of his personal time to ensure experimental work was completed on time.

I would also like to thank Mrs Penny Park-Ross and Ms Soraya von Willingh within the CME lab for their assistance during experimental procedures as well as Ms Sherlyn Gabriel and Mr Richard Curry for their assistance during experimental set-up as well as processing of Digital Image Correlation data.

Table of Contents

<u>I. ABSTRACT</u>	1
<u>II. ACKNOWLEDGEMENTS</u>	2
<u>1. INTRODUCTION</u>	7
1.1 BACKGROUND TO INVESTIGATION	7
1.2 OBJECTIVES OF REPORT AND INVESTIGATION	8
1.3 SCOPE AND LIMITATIONS OF INVESTIGATION	8
<u>2. LITERATURE REVIEW</u>	9
2.1 FUSED DEPOSITION MODELLING	9
2.2 SURFACE IMPROVEMENT TECHNIQUES OF FDM PARTS	11
2.3 CHEMICAL POST-PROCESSING	14
2.4 ANISOTROPY OF FDM PARTS	16
2.5 TENSILE PROPERTIES OF FDM PARTS	16
2.6 DIGITAL IMAGE CORRELATION	19
2.7 SUMMARY	20
<u>3. EXPERIMENTAL METHOD</u>	21
3.1 EXPERIMENTAL SET-UP	21
3.2 MATERIAL, GEOMETRY AND PRINTING OF SPECIMENS	22
3.2.1 MATERIAL USED IN PRINTING	22
3.2.2 SPECIMEN GEOMETRY	22
3.2.3 PRINTING SPECIMENS	25
3.3 CHEMICAL POST-PROCESSING	29
3.3.1 CHEMICAL DIPPING	30
3.3.2 VAPOUR SMOOTHING	31
3.4 SURFACE ROUGHNESS TESTING	32
3.4.1 QUALITATIVE TESTING	32
3.4.2 QUANTITATIVE TESTING	33
3.5 TENSILE TESTING	34
3.6 DIGITAL IMAGE CORRELATION	34

3.7 DATA PROCESSING	35
<u>4. RESULTS</u>	<u>37</u>
4.1 PRINTING	37
4.1.1 TEMPERATURE AFFECTS ON PRINTING	37
4.1.2 PRINTING UPRIGHT SPECIMENS WITHOUT SUPPORT MATERIAL	39
4.2 CHEMICAL POST-PROCESSING	40
4.2.1 MICROSCOPY IMAGES	40
4.2.2 SURFACE ROUGHNESS GRAPHS	44
4.3 TENSILE TESTING	49
4.3.1 SPECIMEN DIMENSIONS	49
4.3.2 STRAIN DATA	49
4.3.3 ENGINEERING STRESS VS. STRAIN GRAPHS	52
4.3.4 TESTING ERRORS	58
4.3.5 DATA FROM STRESS-STRAIN GRAPHS	60
4.3.6 MICROSCOPY IMAGES AFTER FRACTURE	61
<u>5. DISCUSSION</u>	<u>62</u>
5.1 FUSED DEPOSITION MODELLING USING ABS FILAMENT	62
5.2 CHEMICAL POST-PROCESSING	63
5.3 TENSILE TESTING	64
<u>6. CONCLUSION AND RECOMMENDATIONS</u>	<u>68</u>
<u>REFERENCES</u>	<u>70</u>
<u>APPENDIX A: SPECIMEN DIMENSIONS</u>	<u>75</u>
<u>APPENDIX B: ACETONE MEASUREMENTS DURING VAPOUR SMOOTHING</u>	<u>77</u>
<u>APPENDIX C: MATLAB CODE</u>	<u>78</u>
<u>APPENDIX D: BUDGET</u>	<u>89</u>
<u>APPENDIX E: RISK ASSESSMENT</u>	<u>90</u>
<u>APPENDIX F: INTERIM REPORT</u>	<u>91</u>

List of Figures

FIGURE 1: SCHEMATIC OF FDM PRINTER [19].....	9
FIGURE 2: SCHEMATIC OF CHORDAL AND STAIR-CASE EFFECT [14].....	11
FIGURE 3: SCHEMATIC OF THE BUILD ORIENTATION PARAMETER [6].....	12
FIGURE 4: PRINTING PARAMETERS OF FDM PARTS SHOWN FOR EACH LAYER [28].....	12
FIGURE 5: IMPROVEMENT OF SURFACE FINISH FROM RIGHT TO LEFT [HACKADAY].....	13
FIGURE 6: SEM IMAGES OF PARTS BEFORE AND AFTER VAPOUR SMOOTHING [19].....	14
FIGURE 7: SCHEMATIC OF ABS PARTS MADE UP OF LAYERS OF EXTRUDED FILAMENT [21].....	16
FIGURE 8: COMPARISON OF TENSILE RESPONSE ALONG AXIAL, TRANSVERSE AND OUT-OF PLANE DIRECTIONS [20].....	17
FIGURE 9: MICROSCOPIC IMAGES OF UNTREATED AND TREATED PARTS AFTER TENSILE FAILURE [8]	19
FIGURE 10: TRACKING OF A BLOCK OF PIXELS DURING DIC [34].....	20
FIGURE 11: SOLIDWORKS DRAWING OF ASTM D638 TYPE IV SPECIMEN.....	23
FIGURE 12: SOLIDWORKS DRAWING OF ASTM D3039 SPECIMEN.....	24
FIGURE 13: D3039 FRACTURE IN GAUGE SECTION.....	24
FIGURE 14: INCREASED SHELL THICKNESS OF DOG-BONE SPECIMEN.....	26
FIGURE 15: CURA LAYER VIEW MODE OF HORIZONTAL D638 SPECIMEN.....	27
FIGURE 16: CURA LAYER VIEW MODE OF UPRIGHT D3039 SPECIMEN.....	27
FIGURE 17: CURA LAYER VIEW MODE OF UPRIGHT D638 SPECIMEN.....	28
FIGURE 18: SOLIDWORKS DRAWING OF TEST PLATE USED TO OPTIMIZE CHEMICAL POST-PROCESSING	29
FIGURE 19: BATCH 2 SAMPLE 6 MICROSCOPY IMAGE AFTER DIPPING.....	30
FIGURE 20: VAPOUR SMOOTHING EXPERIMENTAL SETUP.....	32
FIGURE 21: WARPING AT GRIPPING SECTION OF SPECIMEN.....	37
FIGURE 22: INITIAL LAYER OF UPRIGHT SPECIMEN AFTER BRIM REMOVED.....	38
FIGURE 23: TOP COVER OF ULTIMAKER PRINTER.....	38
FIGURE 24: UPRIGHT DOGBONE SPECIMEN (A) BOTTOM OF GAUGE SECTION (B) TOP OF GAUGE SECTION.....	39
FIGURE 25: BATCH 2 (A) GAUGE SECTION (B) CORNER OF GRIPPING SECTION (C) NECK.....	40
FIGURE 26: BATCH 3 (A) NECK (B) GRIPPING SECTION.....	41
FIGURE 27: BATCH 5 (A) GRIPPING SECTION (B) NECK (C) EDGE OF GRIPPING SECTION.....	42
FIGURE 28: BATCH 6 (A) NECK OF SPECIMEN (B) SIDE VIEW OF NECK.....	43
FIGURE 29: SURFACE ROUGHNESS GRAPH (BATCH 2 SPECIMEN 2).....	44
FIGURE 30: SURFACE ROUGHNESS GRAPH (BATCH 3 SPECIMEN 2).....	45
FIGURE 31: SURFACE ROUGHNESS GRAPH (BATCH 5 SPECIMEN 1).....	46
FIGURE 32: SURFACE ROUGHNESS GRAPH (BATCH 6 SPECIMEN 1).....	47
FIGURE 33: STRAIN VS. TIME GRAPH FROM DIC (BATCH 1 SPECIMEN 2).....	49
FIGURE 34: TRUNCATED STRAIN VS. TIME GRAPH (BATCH 1 SPECIMEN 2).....	50
FIGURE 35: DIC AND EXTENSOMETER STRAIN VS. TIME GRAPH (BATCH 1 SPECIMEN 2).....	51

FIGURE 36: ENGINEERING STRESS VS. STRAIN FROM EXTENSOMETER (BATCH 1).....	52
FIGURE 37: ENGINEERING STRESS VS. STRAIN FROM DIC (BATCH 1).....	52
FIGURE 38: ENGINEERING STRESS VS. STRAIN FROM EXTENSOMETER (BATCH 2).....	53
FIGURE 39: ENGINEERING STRESS VS. STRAIN FROM DIC (BATCH 2).....	53
FIGURE 40: ENGINEERING STRESS VS. STRAIN FROM EXTENSOMETER (BATCH 3).....	54
FIGURE 41: ENGINEERING STRESS VS. STRAIN FROM DIC (BATCH 3).....	54
FIGURE 42: ENGINEERING STRESS VS. STRAIN FROM EXTENSOMETER (BATCH 4).....	55
FIGURE 43: ENGINEERING STRESS VS. STRAIN FROM DIC (BATCH 4).....	55
FIGURE 44: ENGINEERING STRESS VS. STRAIN FROM EXTENSOMETER (BATCH 5).....	56
FIGURE 45: ENGINEERING STRESS VS. STRAIN FROM DIC (BATCH 5).....	56
FIGURE 46: ENGINEERING STRESS VS. STRAIN FROM EXTENSOMETER (BATCH 6).....	57
FIGURE 47: ENGINEERING STRESS VS. STRAIN FROM DIC (BATCH 6).....	57
FIGURE 48: PERIMETER FRACTURE (BATCH 1 SPECIMEN 6).....	58
FIGURE 49: INADEQUATE SPECKLE PATTERN (BATCH 3 SPECIMEN 5).....	59
FIGURE 50: FRACTURED FACES (A) BATCH 1 (B) BATCH 2 (C) BATCH 3 (D) BATCH 4 (E) BATCH 5 (F) BATCH 6.....	61

List of Tables

TABLE 1: TESTING MATRIX FOR INVESTIGATION.....	21
TABLE 2: CURA PRINTING PARAMETERS	26
TABLE 3: SURFACE ROUGHNESS VALUES	48
TABLE 4: RESULTS FROM STRESS-STRAIN CURVES	60

1. Introduction

This project aims to investigate the effects that chemical post-processing has on an acrylonitrile-butadiene-styrene (ABS) part that has been additively manufactured through the process of Fused Deposition Modelling (FDM). The in-plane and interlaminar tensile properties of treated and non-treated parts were tested in order to determine the extent to which chemical exposure improved the surface of an FDM part as well as how much it altered its strength properties.

1.1 Background to investigation

FDM is a widely used rapid prototyping technique and is increasingly being used to fabricate parts with complex geometries. FDM is advantageous over traditional manufacturing methods due to its ability to manufacture complex geometries in a short time period without extra tooling required, however, printed parts suffer from a poor surface finish. Post-processing treatments are therefore used to smooth the surface of printed parts.

FDM is a relatively new manufacturing method and therefore limited published data is available on the mechanical properties of FDM parts, especially the strength of parts that have undergone post-processing treatments. This investigation will therefore provide new data that will lead to improved design guidelines and more accurate material properties of FDM parts.

1.2 Objectives of report and investigation

The objectives are to:

- Conduct a literature review on previous investigations pertaining to chemical post-processing as well as tensile testing of FDM parts.
- Develop the experimental details and testing methods followed within this investigation.
- Describe the results obtained from testing.
- Draw conclusions on the effectiveness of the post-processing techniques used to smooth parts as well as the effect of chemical exposure on the tensile properties of parts.
- Discuss limitations and constraints within the investigation.
- Make recommendations for future research regarding this investigation.

1.3 Scope and limitations of investigation

This investigation focussed only on chemical treatment as a post-processing technique for 3D printed parts. Parts were printed using the technique of Fused Deposition Modelling and ABS as the filament material. The modelling and printing parameters were kept constant for each print orientation – the x- and z-directions. The differing print orientations allowed for in-plane and interlaminar tensile testing to be performed and therefore in-plane and interlaminar tensile strengths for both treated and untreated parts were investigated and compared. Strain values were calculated using readings from an extensometer as well as data measured using Digital Image Correlation. The results from both techniques were used to plot engineering stress versus strain graphs that could be compared against each other.

2. Literature Review

Additive manufacturing is a “process of joining material to make parts...layer upon layer” [1] and has become an important area in the manufacturing of custom parts in recent years [2]. Three-dimensional printing techniques, which include Stereolithography, Selective Laser Sintering, Ballistic Particle Manufacturing and FDM [3], allow for flexibility within design and manufacturing as well as an absence of tooling and thus have become a competitor for traditional manufacturing techniques. Single, functional parts with complex geometries can be produced in a short amount of time, at a relatively low cost, which therefore significantly reduces the product development cycle of a prototype and enables rapid feedback for an improved design process. Rapid prototyping does however, have certain limitations pertaining to large-scale manufacturing, economic constraints and limited mechanical performance of printed parts. [4]

2.1 Fused Deposition Modelling

The printing technique of FDM, invented and patented by Stratasys Inc., is one of the most popular additive manufacturing processes which involves the extrusion of thermoplastic filaments by a movable head, in a precoded pattern in the x and y-direction, onto the build platform which moves incrementally in the Z direction for each new layer [5] – as seen in Figure 1.

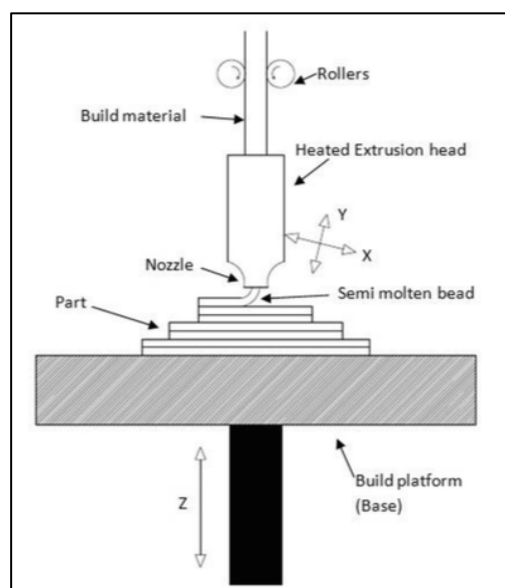


FIGURE 1: SCHEMATIC OF FDM PRINTER [19]

A 3D model, created using Computer Aided Design (CAD) software is converted into G-code instructions that control the extruder heat and build plate of the printer as well as their temperatures and the extrusion rates required. The filament material is heated to a molten state within the extruder head, which then solidifies and adheres to the previous layer following deposition. The thickness of each layer is controlled by the height at which the head deposits material onto the previous layer [5].

The popularity of FDM is due to user-friendly desktop printers – such as the RepRap printer, employing FDM to fabricate specimens [6]. It is estimated that the number of RepRaps in use has increased from 4 to 4500 between 2008 and 2011 [7]. Materials used in FDM are also popular in engineering activity, namely the recyclable thermoplastics acrylonitrile-butadiene-styrene (ABS) and polycarbonate (PC) [8]. These materials are required to have a suitable melt viscosity which is high enough to maintain the structural integrity of the part when in use and low enough to be extruded during printing [9].

In order for signals to be generated for the printer, the 3D CAD model must be converted into a Standard Triangulation Language (STL) file format, which “describes the surface geometry of an object as a tessellation of triangles” [1] so that the part geometry can be transferred into computer code. The STL file is then sliced into horizontal layers of the part using slicing software whereby the tool path of the extruder head is generated for each layer [10].

2.2 Surface improvement techniques of FDM parts

The STL file format causes a poor surface finish of printed parts because part surfaces are approximated as a series of triangles, as stated above. This is known as the 'chordal effect', which occurs because the curved surfaces of a part are approximated as linear surfaces [10]. Increasing the tessellation resolution would result in smaller triangles being used to approximate the surface and therefore reducing the chordal effect, but longer printing times and larger processing files would also result [11]. Slicing the part into layers further causes a poor surface finish known as the 'stair-case effect' whereby ridges appear along the surface of the part, as shown in Figure 2.

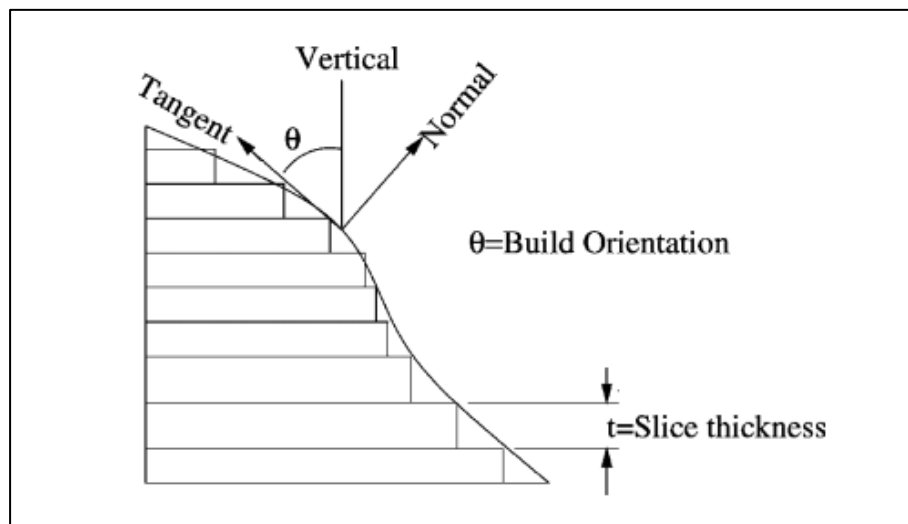


FIGURE 2: SCHEMATIC OF CHORDAL AND STAIR-CASE EFFECT [14]

Galantucci et al. [12] states that decreasing the layer/slice thickness would reduce the stair-case effect because the distance between adjacent layers would be reduced. Decreasing layer thickness, however, increases the printing time of a part because the part then consists of more layers for the same print.

Lan et al. [13] determined how the stepped surface could be smoothed by different build orientations, which are shown in Figure 3.

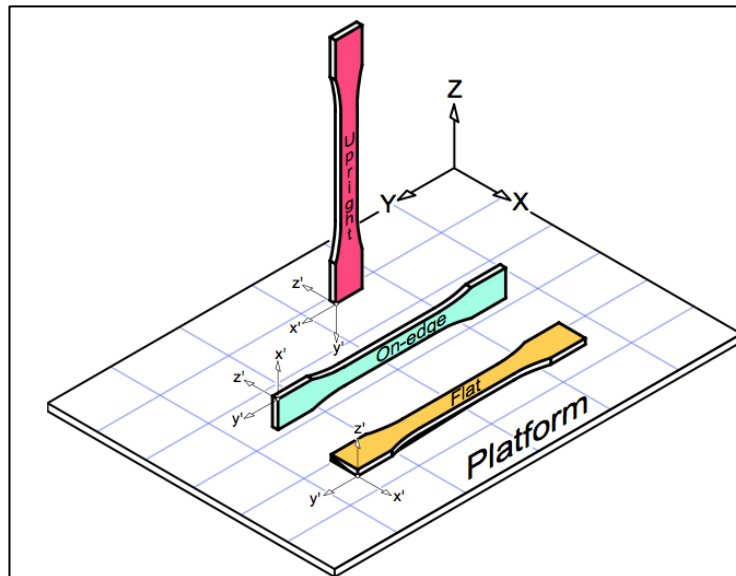


FIGURE 3: SCHEMATIC OF THE BUILD ORIENTATION PARAMETER [6]

The conclusion was made that orientations whereby the horizontal and vertical faces of a part are maximized and support requirements are minimized will reduce the stair-case effect [13]. This is because horizontal faces lie on the non-stepped surfaces and the vertical faces lie parallel to the vertical axis of the part.

Other methods to improve surface finish include the optimization of fabrication parameters, which are associated with deposition of the extruded filament, as shown in Figure 4. The seam line between filaments and layers degrades surface finish and therefore filament width and air gap are found to have a large effect on the surface finish of an FDM part [12].

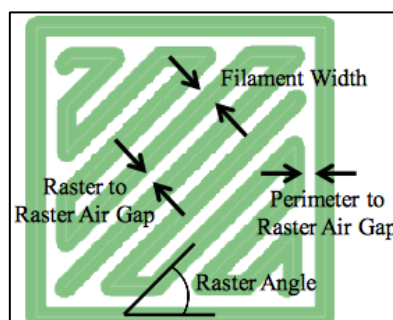


FIGURE 4: PRINTING PARAMETERS OF FDM PARTS SHOWN FOR EACH LAYER [28]

Post-printing treatments are used if altering the printing parameters, as discussed above, is not successful in achieving a required surface finish. Post-processing methods include hot cutter machining; whereby an increased tool temperature temporarily softens the part so that ridges on the part can be machined [14], thermal processing, which alters the crystallinity of a printed part [30] and chemical post-processing.

The surface finish of a prototype has aesthetic importance because its function is to display a design or concept and therefore needs to be appealing to the eye. More precise dimensions also result from a smoother surface, which improve assembling and operational performance as well as increase surface life [13]. The improved surface finish of a prototype is shown in Figure 5.



FIGURE 5: IMPROVEMENT OF SURFACE FINISH FROM RIGHT TO LEFT [HACKADAY]

2.3 Chemical post-processing

Chemical post-processing is suitable for smoothing complex surfaces and is advantageous over other techniques because it is independent of the skill of a worker and is relatively inexpensive [12] although, smoothing requires a suitable solvent that will react with the extruded material. The filament material, which is predominantly used for chemical treatments, is ABS as it has a lowered reticulation degree, having weak interactions with polar solvents. Jin et al. [15] states that the reaction between PLA and the solvent, dichloromethane (methylene chloride) is difficult to control whereas, the polar solvent dimethyl ketone (acetone) easily dissolves ABS. Acetone is also low in cost and toxicity and has high diffusivity [12].

Chemical exposure to FDM parts causes temporary, localised melting of surface layers which therefore causes material to flow “from peaks and deposit into valleys” [19] of the surface, as shown in Figure 6. Layers therefore settle as a smoother surface following chemical exposure as the ‘stair-case’ gap is filled between adjacent filaments.

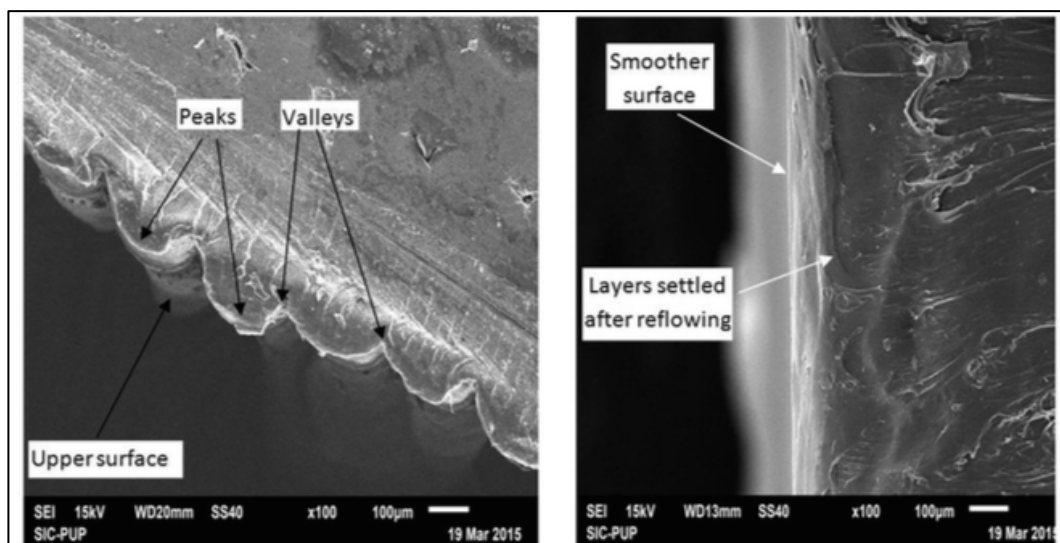


FIGURE 6: SEM IMAGES OF PARTS BEFORE AND AFTER VAPOUR SMOOTHING [19]

Chemical treatments involve the use of chemicals in liquid or vapour phases. Galantucci et al. [12] investigated how acetone dipping affects the surface roughness of an ABS FDM part. Parts were submerged for 300 seconds in a solution of 90% acetone and 10% water as the process was stated to be difficult to control when using pure acetone. The average surface roughness (Ra) measured on the top surface of each part was significantly reduced using this solution from 11.8 μm to 2.2 μm for a slice height of 0.178mm and 17.2 μm to 4.6 μm for a slice height of 0.254mm. Galantucci et al. [12] also concluded that the stair-case effect was reduced by acetone dipping.

Havenga et al. [16] however, submerged specimens in pure acetone for a shorter time period of 10 seconds in order for a more “aggressive infiltration” [16] of acetone into the ABS part. This method was also successful in reducing the Ra value from 17.4 μm to 2.3 μm for parts printed horizontally with a layer thickness of 0.2mm and, with the same printing parameters, from 1.6 μm to 0.4 μm for parts printed vertically. Havenga et al. [16] also investigated vapour smoothing whereby pure acetone was enclosed in a chamber with a printed part for 10 seconds at a temperature of 60°C. The effect of vapour smoothing reduced the Ra value of horizontally printed parts from 17.4 μm to 0.2 μm and vertically printed parts from 1.6 μm to 0.2 μm . The method of vapour smoothing was therefore more effective within this investigation and horizontally printed parts experienced more smoothing than vertically printed parts.

Vapour smoothing involves techniques modelled on the Vapour Smoothing Station (VSS), patented by Stratasys Inc., whereby FDM parts are hung inside a heating unit subjecting the outer surfaces of the part to heated chemical vapours [17]. When heated, the acetone vapours vaporize to a larger extent and react with the surface layers of the hanging part [19]. Singh et al. [18] investigated the use of a VSS and heated acetone to smooth ABS parts with cubic, cylindrical and hemispherical geometries. Surface roughness measurements were found to be reduced to a nano-level without affecting the dimensional accuracy of the part. Although, Scanning Electron Microscopy (SEM) analysis showed that prolonged smoothing led to part deterioration and therefore an optimal exposure time of 20 seconds was required within this investigation.

2.4 Anisotropy of FDM parts

FDM parts are anisotropic which means that when tested in different pull directions; the mechanical properties of a printed part will differ [20]. Its anisotropic nature is due to the method in which FDM parts are fabricated. Layers of extruded filament mechanically adhere to adjacent layers upon solidification. The mechanical bonds between layers have a lower strength than bonds within polymeric chains along each filament [21]. This structure is shown in Figure 7.

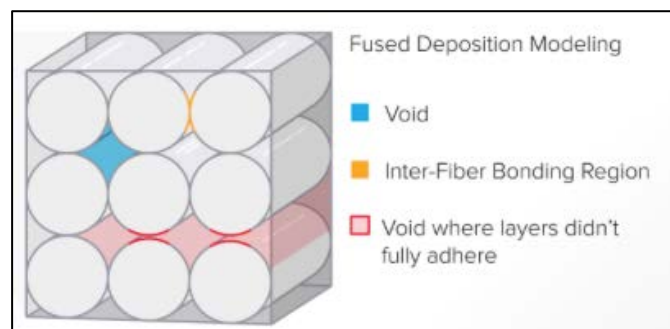


FIGURE 7: SCHEMATIC OF ABS PARTS MADE UP OF LAYERS OF EXTRUDED FILAMENT [21]

The forces required to fracture a part between its layers will therefore be lower than the forces required to fracture a part along its filaments. Tensile strengths can thus be stated as direction dependent [20].

2.5 Tensile properties of FDM parts

Many previous studies have focussed on the tensile properties of FDM parts. Tymrak et al. [7] investigated the tensile strength and elastic modulus of both ABS and PLA ASTM D638 printed parts for differing printing parameters – at a crosshead rate of 5mm/min. Layer heights of 0.2mm, 0.3mm and 0.4mm were included as well as raster angles in the 0°/90° orientation and 45°/-45° orientation. The layer height of 0.2mm produced the greatest tensile strength – 29.7MPa for ABS specimens, while 0.4mm produced the greatest elastic modulus, 1.875GPa for ABS specimens. Specimens with a layer height of 0.2mm had an average elastic modulus of 1.839GPa. The 0°/90° orientation was found to have the highest strength whereas the 45°/-45° orientation had the greatest elastic modulus. However, these orientations also contained perimeter lines at 0°. The assumption was therefore made during the investigation that the number of perimeter lines would have an effect on the strength of the part – as perimeter lines increase the number of

unidirectional filaments that are aligned with the pull direction of the specimen. This study of focussing on increased unidirectional filaments led Song et al. [20] to investigate the anisotropy of 3D-printed parts.

A part's anisotropy and its effects on tensile properties were investigated by cutting dog-bone specimens out of 3D-printed PLA blocks – where the extruded filaments were unidirectional, and testing them in the axial, transverse and out-of-plane directions. Song et al. hypothesised that the “interfaces between adjacent layers are likely to possess different material properties from those of the bulk of the layers” [20] and from results obtained concluded that the axial strength along filaments is higher than the out-of-plane strength as shown in Figure 8. Furthermore, the out-of-plane direction was found to be more brittle than the other testing directions.

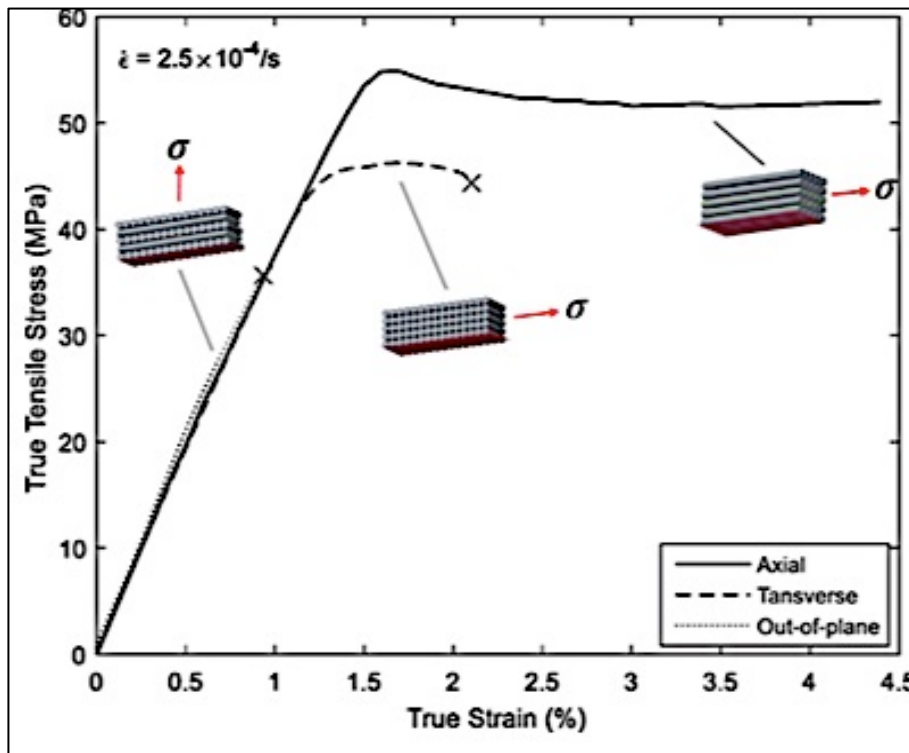


FIGURE 8: COMPARISON OF TENSILE RESPONSE ALONG AXIAL, TRANSVERSE AND OUT-OF-PLANE DIRECTIONS [20]

The anisotropic nature of FDM specimens was verified by Alaimo et al. [31], whereby the effects of fibre orientation and filament dimensions on the mechanical properties of ABS parts was investigated. The ASTM D3039 standard was used, instead of the ASTM D638 standard, as it was stated to be “tailored to anisotropic materials” [31] whereas dog-bone specimens had previously prematurely failed at stress

concentrations on the radii of the part. Tabs were also adhered to the ends of each specimen to avoid gripping damage. Testing showed that longitudinal specimens with a 0° fibre orientation behaved in a ductile manner – undergoing large plastic deformation before fracturing, while transverse specimens with a 90° fibre orientation behaved in a brittle manner – undergoing almost no plastic deformation. The Young's modulus for longitudinal specimens was also found to be higher than that of transverse specimens – 1.953GPa and 1.752GPa, respectively.

Sood et al. [22] investigated how the strength of FDM parts is affected by the printing variables that the strength is stated to be primarily dependent on. These included build orientation, layer thickness, raster angle, raster width and air gap between filaments. The tensile strength at break was tested according to the ISO R527:1966 standard at a rate of 1mm/s. Following tensile testing the conclusions were made that a smaller raster angle allows for filaments to be inclined along the direction of loading therefore inducing forces along the filament. This will lead to an increased strength of the part as loading is in the axial direction. A smaller air gap will also create a stronger bond between adjacent filaments and layers, which will in turn increase the tensile strength of the part in all loading directions.

Galantucci et al. [8] investigated the influence of chemical treatment on the tensile and flexural strength of FDM parts. Tensile tests were conducted as per the ISO 527:1997 standard at 1mm/min and each specimen had a layer height of 0.254mm. As previously mentioned, the treatment method involved dipping specimens in an acetone solution. Figure 9 shows how this chemical treatment dissolved individual filaments that then joined together in a molten state and resolidified.

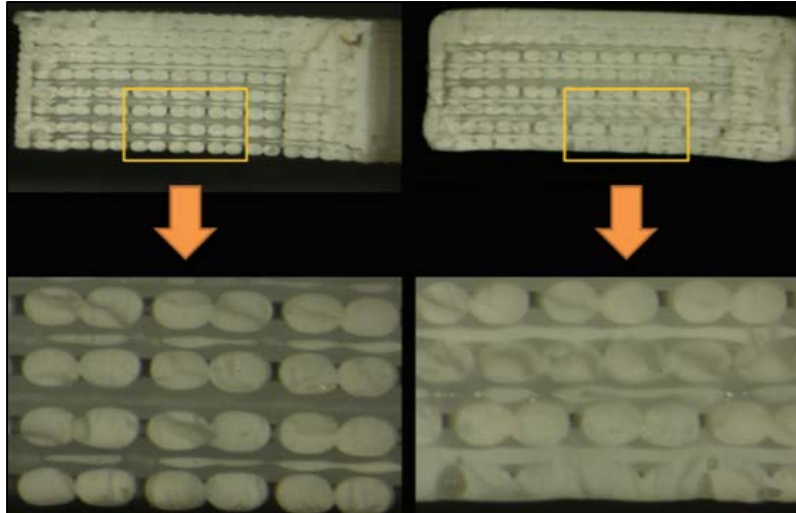


FIGURE 9: MICROSCOPIC IMAGES OF UNTREATED AND TREATED PARTS AFTER TENSILE FAILURE [8]

With longer chemical treatment times; the maximum displacement of the part was improved – from 2.85mm for untreated specimens to 2.98mm for treated specimens, but the maximum stress that the part could withstand decreased – from 19.8MPa for untreated specimens to 17.59MPa for treated specimens. The increased displacement meant that treated parts had a higher ductility due to greater adhesion between fibres. It was also stated that chemical treatment improves the isotropy of a part whereby “the angle of filaments loses its influence on the mechanical properties” [8].

2.6 Digital Image Correlation

Digital Image Correlation (DIC) is a “non-contact optical technique” [32] that is used to measure strain and displacement. Surface displacement measurements are obtained by tracking blocks of pixels in a region of interest (ROI) through the comparison of digital photographs taken consecutively during deformation – as shown in Figure 10, from which strain maps can be created. One or more cameras are used depending on whether analysis is conducted in 2 or 3-dimensions [33]. Pixel blocks within the ROI are required to be random, unique and highly contrasted in order for DIC to effectively track and measure deformation [32].

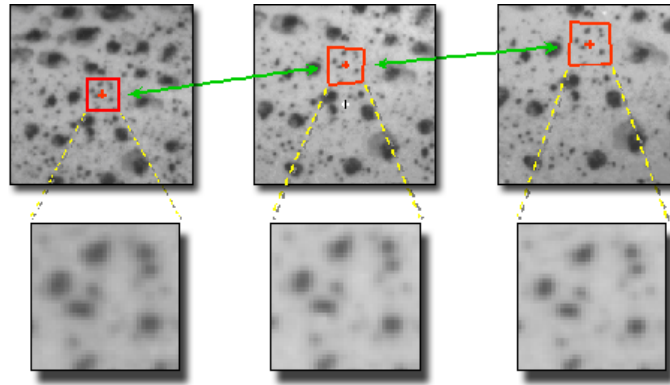


FIGURE 10: TRACKING OF A BLOCK OF PIXELS DURING DIC [34]

DIC testing done by Lin [33] simultaneously with conventional strain gauges during tensile tests validated the accuracy of results obtained by DIC. It was further concluded that DIC is capable of full-field deformation measurements, which allows for greater flexibility in measuring strain, whereas contact methods such as strain gauges have physical restraints. DIC is also advantageous over other non-contact methods such as electronic speckle pattern interferometry (ESPI) as it is less expensive and will maintain its accuracy when used outside of the laboratory - requiring less precision during setup [32].

2.7 Summary

This chapter has reviewed and discussed the following items, relevant to this investigation:

- The additive manufacturing technique of Fused Deposition Modelling.
- Techniques to improve the surface finish of FDM parts including optimising printing parameter and post-printing treatments.
- Chemical post-processing as a post-printing treatment.
- The need to test FDM parts in different pull directions because of their anisotropic nature.
- The tensile properties of FDM parts and how they are affected by different printing parameters as well as chemical treatments.
- The technique of Digital Image Correlation and its advantages over other displacement and strain measurement techniques.

3. Experimental Method

3.1 Experimental set-up

The testing matrix for this investigation is shown in Table 1. Two test plates were initially printed that were used to optimize the chemical exposure time of specimens that underwent chemical post-processing.

TABLE 1: TESTING MATRIX FOR INVESTIGATION

Batch	Test	Testing Geometry	Build orientation	Post-processing
-	1	Test plate	X-direction	Chemical dipping
-	2	Test plate	X-direction	Vapour smoothing
1	3-9	D638 Type IV	X-direction	-
2	10-16	D638 Type IV	X-direction	Chemical dipping
3	17-23	D638 Type IV	X-direction	Vapour smoothing
4	25-30	D638 Type IV	Z-direction	-
5	32-37	D638 Type IV	Z-direction	Chemical dipping
6	38-44	D638 Type IV	Z-direction	Vapour smoothing

Batch 1 and 4 consisted of seven D638 Type IV specimens printed in the x-direction and z-direction, respectively. They were not chemically post-processed; the strength data obtained from these specimens was used as a benchmark against which to compare the strength data of chemically treated specimens. A minimum value of five specimens should be tested for each build direction in order to comply with ASTM testing standards [24] and therefore, in order to account for possible errors within the investigation, seven specimens for each batch were fabricated.

3.2 Material, geometry and printing of specimens

Specimens used within this investigation were 3D-printed using an Ultimaker 2 and Ultimaker 2+ desktop printer, which are property of the Mechanical Engineering department at the University of Cape Town, using the G-code flavour RepRap (Marlin/Sprinter). Specimens were initially designed as Solidworks models and then printed through the process of Fused Deposition Modelling using the slicing software and G-code generator, Cura.

3.2.1 Material used in printing

The filament material used in the extrusion process was ABS as it can be heated, extruded and solidified without significant degradation. Its counterpart, PLA has superior mechanical properties to ABS but ABS was used for the practical reason that it is easily chemically post-processed using the highly volatile solvent, acetone [12]. ABS, like PLA, is also readily available in filament form and is recyclable – thus an environmentally friendly plastic.

3.2.2 Specimen geometry

The American Standard for Testing and Materials (ASTM) was followed to determine testing geometries and methods for tensile testing. The D638 standard for Type IV tensile specimens [24] was followed to determine the in-plane tensile properties of each part [23]. The dimensions for the test specimen are shown in Figure 11. Type IV dimensions were used so that the length and thickness of the specimen were reduced for reduced printing time.

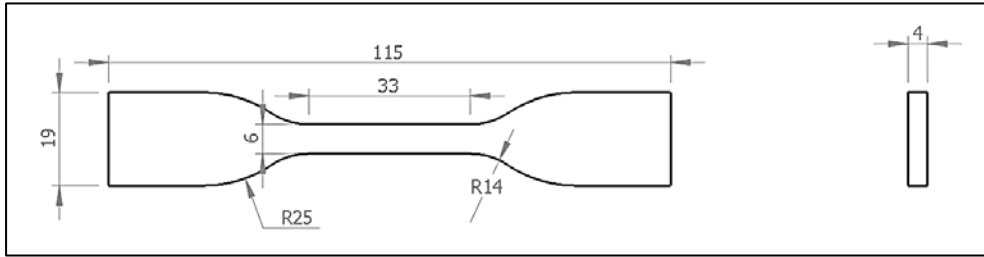


FIGURE 11: SOLIDWORKS DRAWING OF ASTM D638 TYPE IV SPECIMEN

The Type IV geometry also permitted a large outer radius of the specimen (25mm), which reduced stress concentrations caused by changes in filament deposition direction. The dog-bone shape is preferential as it ensures that fracture occurs in a specified area along the gauge length, where the width of the part narrows.

In order to test for interlaminar tensile properties of a printed part, due to printed parts being anisotropic in nature – specimens needed to be tested whereby the pull direction was perpendicular to the layers of the part so that the specimen was placed under interlaminar tension. This testing geometry was obtained by printing in the z-direction thus orientating the part upright. Printing a dog-bone specimen standing upright was suspected to be problematic due to overhangs at the narrowing gauge section. Therefore, the ASTM D3039 standard testing geometry [25] for straight-sided tensile specimens was initially followed [26]. This geometry would be easy to print upright it would have no overhangs and consequently require no support material during printing. The dimensions for the test specimen are shown in Figure 12. Deviations from the standard occurred by reducing the overall length of the specimen in order to reduce printing time, which would not have an affect on the strength data obtained, and increasing the thickness to 4mm – so that thickness was kept constant for both testing directions.

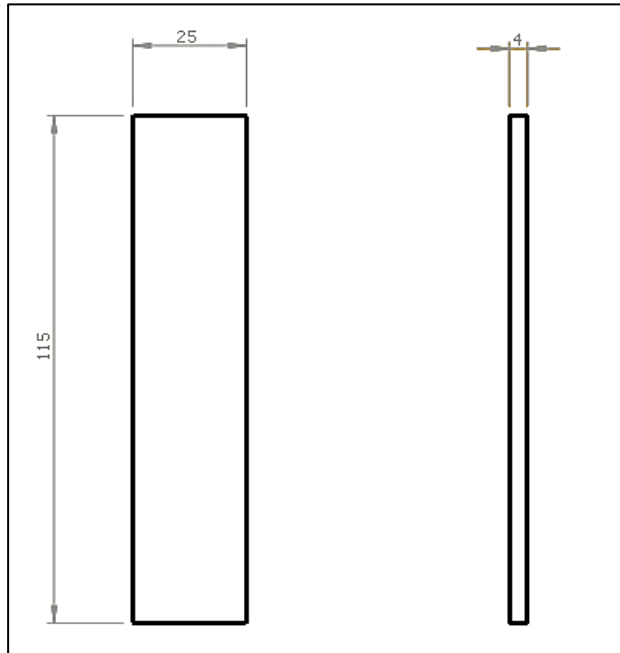


FIGURE 12: SOLIDWORKS DRAWING OF ASTM D3039 SPECIMEN

However, after placing a printed D3039 specimen under tension within the Zwick tensile tester, the straight-sided specimen fractured within the gripping section – as shown in Figure 13.



FIGURE 13: D3039 FRACTURE IN GAUGE SECTION

Tab adherence is strongly recommended for testing D3039 unidirectional materials until fracture in the filament direction [25] and are adhered to specimens in order to reduce gripping damage from the grips as well as produce failure within the created gauge section – between the tabs. Tab adherence is however difficult and introduces more stress concentrations into the specimen if not adhered correctly. It can therefore be difficult to evaluate whether a D3039 specimen has fractured due to an introduced stress concentration or whether the fracture point was indeed the weakest part of the specimen.

Printing D638 Type IV specimens upright, in the z-direction, was therefore investigated as a more preferable option with regards to interlaminar testing. Although, during printing it needed to be ensured that overhangs within the part could support themselves and not sag without support material.

3.2.3 Printing specimens

In order to print specimens – SolidWorks models were exported as STL files so that they could be read by the slicing software, Cura. Although printing parameters are stated to affect surface finish and tensile properties of a part, the print settings were kept constant for each test geometry so that only the variable of chemical finishing on tensile properties was investigated. Table 2 shows the parameters inputted into Cura for the horizontal and upright D638 test geometries as well as the tested upright D3039 test geometry – using ABS as the filament material. These settings have been specified by Cura instructions as well as Dr. Govender - optimized from printing experience.

ABS has a glass transition temperature of 105° [27], therefore the extruder head set at a temperature of 255°C ensured the filament was in a semi-molten state. The bed of the printer was set at 98°C so that the extruded filament would adhere to the bed after deposition. In order to further ensure this, an ABS slurry was applied to the printer bed, which would soften at the print bed temperature and act as an adhesive for the initial printed layer. Spraying acetone onto the bed and then rubbing an ABS puck onto the acetone so that the ABS melted and resolidified onto the bed achieved this slurry.

TABLE 2: CURA PRINTING PARAMETERS

Settings	Value		
	D638	D3039	D638
Layer height (mm)	0.2	0.2	0.2
Fill density (%)	100	100	100
Raster angle (°)	45	45	45
Print speed (mm/s)	50	50	50
Print temperature (°C)	255	255	255
Bed temperature (°C)	98	98	98
Filament diameter (mm)	2.85	2.85	2.85
Nozzle size (mm)	0.4	0.4	0.4
Shell thickness (mm)	2.4	1.2	1.2
Build orientation	X-direction	Z-direction	Z-direction

In-plane tensile testing required that filaments were unidirectional so that when the part was axially loaded, filaments in the gauge section were in pure tension - as shown in Figure 14. In order to obtain a unidirectional filament pattern for the dog-bone specimen, the shell thickness (perimeters) was increased from 1.2mm to 2.4mm for in-planes specimens, which reduced the area of the 45° infill pattern for each layer.

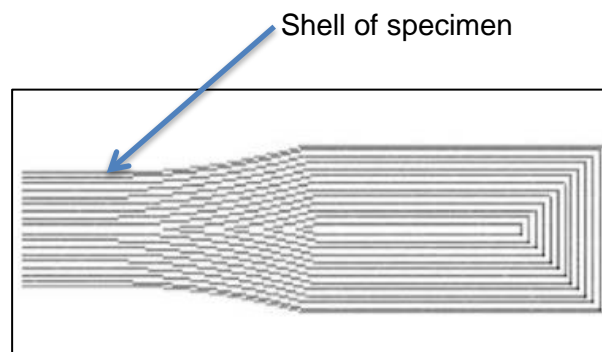
**FIGURE 14: INCREASED SHELL THICKNESS OF DOG-BONE SPECIMEN**

Figure 15 shows the Cura layer view mode for the dog-bone specimen printed in the x-direction. The shell thickness of 2.4mm further ensured that the gauge section was not entirely made up of unidirectional filaments but some infill was still present in each layer, so that part distortion did not occur whereby adjacent unidirectional perimeters at the centre of the part raised – causing part distortion for subsequent layers. The estimated printing time was 52 minutes using 0.97 metres of filament (20 layers).

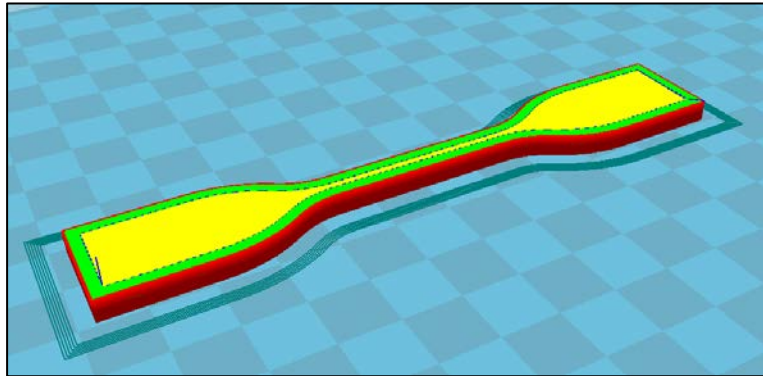


FIGURE 15: CURA LAYER VIEW MODE OF HORIZONTAL D638 SPECIMEN

Figure 16 shows the Cura layer view mode for the rectangular coupon specimen. The shell thickness was set to 1.2mm because testing was between layers with a 100% fill density, and therefore the filament direction within each layer was not important. The estimated printing time was 1 hour 35 minutes using 1.86 metres of filament (575 layers).

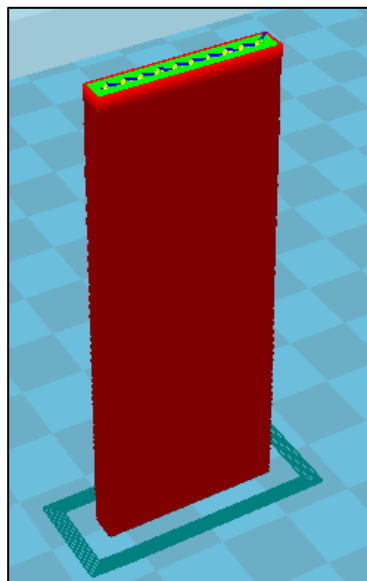


FIGURE 16: CURA LAYER VIEW MODE OF UPRIGHT D3039 SPECIMEN

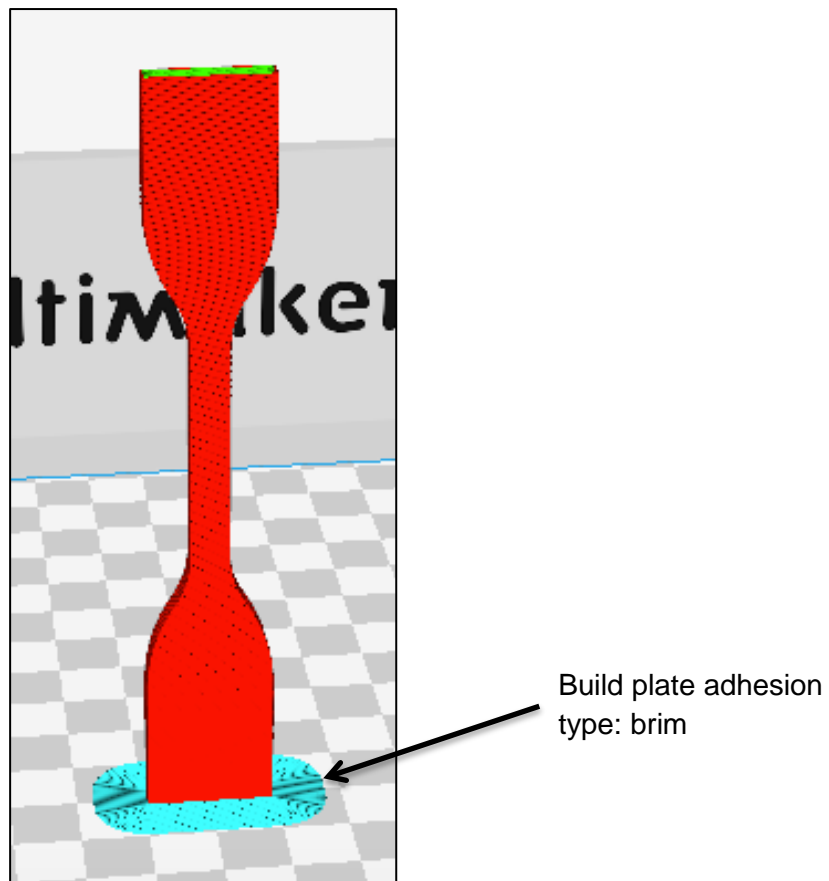


FIGURE 17: CURA LAYER VIEW MODE OF UPRIGHT D638 SPECIMEN

The upright dog-bone specimens were printed using the updated Ultimaker 2+ printer; the Cura layer view mode is shown in Figure 17. The estimated printing time was 48 minutes using 0.96 metres of filament (575 layers). The build plate adhesion type was also changed from skirt to brim. Skirt lines were initially used as a check before printing the specimen, regarding filament adhesion to the plate and extrusion. A brim, however, deposits lines around the base of the printed specimen, creating a larger surface area onto the print bed. This is recommended when printing with ABS as it enhances adhesion to the plate and therefore reduces warping by resisting pulling forces during cooling of the specimen [35].

3.3 Chemical post-processing

Parts underwent chemical treatments after printing to smooth their surfaces and reduce the 'stair-case' and 'chordal' effects produced during FDM as well as the seam lines between filaments and layers. Within this investigation, two different chemical treatment methods were used, namely chemical dipping and vapour smoothing.

Before the printed specimens were chemically treated, two test parts with the geometry shown in Figure 18 were be printed and chemically smoothed using each method so that exposure times could be optimised. This ensured that the tensile specimens were not overexposed to acetone and thus damaged.

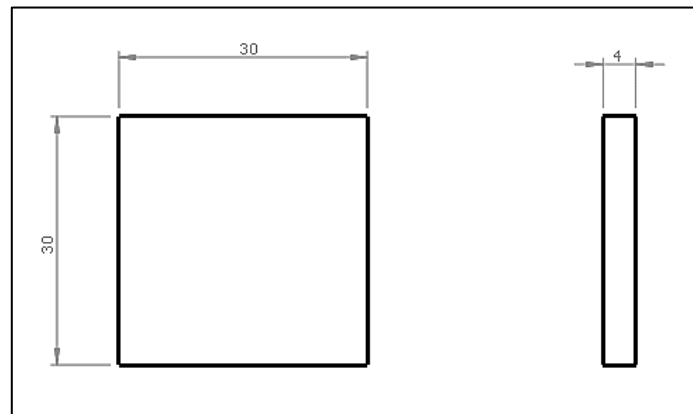


FIGURE 18: SOLIDWORKS DRAWING OF TEST PLATE USED TO OPTIMIZE CHEMICAL POST-PROCESSING

Each test plate was estimated to take 33 minutes to print using 0.58 metres of filament (20 layers). The same printing parameters and thickness were used as before.

3.3.1 Chemical dipping

Specimens were chemically dipped by submerging the part into a 'bath' of liquid. The bath contained a solution of 90% Acetone and 10% distilled water [8] so that the smoothing process was controllable and not aggressive.

A glass beaker (not reactive with acetone) was filled with 300ml of acetone and 33ml of distilled water so that the liquid level was high enough to completely submerge the specimen. Although, during testing the beaker needed to be re-filled with acetone and distilled water in the correct ratio due to acetone having a high evaporation rate because of weak intermolecular forces [12]. Each specimen was initially dipped 4 consecutive times for 20 seconds and then left to dry on tin foil – to prevent sticking onto a surface. They were redipped for 35 seconds each and then dipped again while agitating the solution for 35 seconds. This experimental approach on dipping specimens was followed based on how the specimens were reacting to the acetone and whether they had smoothed adequately. Agitation of the acetone solution caused a greater smoothing effect on the specimens than previous rounds of dipping.

Tongs were used to dip specimens but the force exerted by the tongs on the surface of specimens led to indentations after they had been exposed to acetone and therefore had softened – as shown in Figure 19. Although, specimens were not gripped in the gauge section and therefore no deformation occurred within this area.

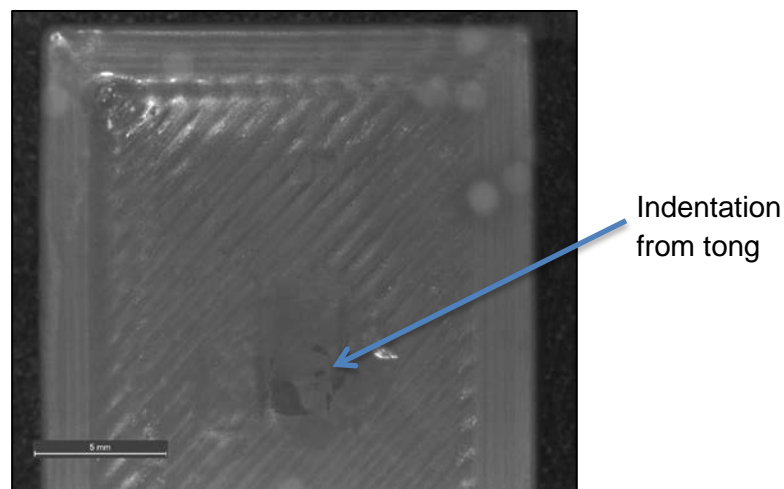


FIGURE 19: BATCH 2 SAMPLE 6 MICROSCOPY IMAGE AFTER DIPPING

3.3.2 Vapour smoothing

A Polypropylene (PP) container was used to enclose acetone vapours within an environment containing ABS specimens so that the surrounding vapours would smooth the specimens. Polypropylene was used as it does not react with acetone [36]. Tin foil was laid at the bottom of the container for specimens to be placed on so that they would not stick to the container floor when subjected to acetone vapours. Although, if subjected to the vapours for too long – the specimens melted and therefore stuck to the tin foil.

Cold vapour smoothing was initially conducted by soaking paper towel in acetone and hanging it over the sides of the container – being held down by the lid. Specimens were contained inside this environment for 40 minutes but did not experience any smoothing effects. It was concluded that the paper towel was absorbing most of the acetone and therefore not enough vapours were present in the container to then smooth the specimens.

A second method to conduct vapour smoothing was followed whereby a beaker of acetone was placed into the container alongside the specimens. Although, the beaker's surface area was relatively small, thus only allowing a small amount of acetone to diffuse into the container volume. This method was therefore also unsuccessful in adequately smoothing specimens.

Lastly, acetone was poured into a petri dish – which had a larger surface area than the beaker, and placed into the container, which sat on a magnetic stirrer so that the acetone within the dish could be agitated – as shown in Figure 20. Agitation accelerates the diffusion process and therefore increases the vapour concentration within the container. The rate of the magnetic stirrer was set to 650l/min and the extent of evaporation was measured by finding the difference in mass of the petri dish filled with acetone liquid before and after smoothing – measurements are shown in Appendix B. Although, when agitated, the stirring piece within the petri dish caused some acetone to splash out onto the tin foil – affecting these readings. The vapour exposure time was decided upon experimentally depending on how the test plate reacted with the vapours throughout the exposure period, which led to a test time of 1 hour 30 minutes.



FIGURE 20: VAPOUR SMOOTHING EXPERIMENTAL SETUP

3.4 Surface roughness testing

The effects of chemical post-processing on specimens printed in both the x and z-directions were examined qualitatively as well as quantitatively with regards to the surface roughness of the specimens.

3.4.1 Qualitative testing

Qualitative testing has great importance, as the reason for smoothing parts is to improve the overall appearance of a printed specimen. Each specimen was therefore primarily examined with the naked eye before and after post-processing to judge how much of an effect post-processing had on the surface finish of the part. This gave an estimate of how successful each testing method was and whether the goal of improving the appearance of each specimen was achieved.

Microscopic images were also taken which enabled images to be examined with a higher degree of detail. At a microscopic level, the individual filaments of a specimen could be viewed. Images after chemical treatment were assessed to determine whether acetone dipping and vapour smoothing had an effect on the surface filaments of a part.

3.4.2 Quantitative testing

Data was recorded, regarding the surface profile of each specimen's gauge section, using a contact profilometer whereby the surface roughness of the specimen was quantified. The diamond stylus of the profilometer moved 25mm along each specimen's gauge length at a rate of 0.25mm/s. The surface variations in the y-direction were then measured as a function of stylus position in the x-direction – sampling at 200Hz. X versus Y plots, in micrometres, showed the surface topography of each specimen's gauge length [37].

The one-dimensional surface roughness parameter (Ra) was calculated for each specimen using Equation 1. As described in the ASME B46.1 standard, this value shows the average roughness of the surface of the specimen and is calculated by integrating the absolute value of the surface profile height function over a given evaluation length [38].

$$Ra = \left(\frac{1}{L}\right) \int_0^L |Z(x)| dx \quad [1]$$

Where $L = \text{evaluation length } (\mu\text{m})$

$Z(x) = \text{profile height function}$

Although, as the displacement data did not easily fit a profile height function, the integral was rather approximated using the Trapezoidal rule as shown in Equation 2 [39], using height deviations from the mean line.

$$Ra = \frac{1}{N} \sum_{i=1}^N |y_i| \quad [2]$$

Where $N = \text{number of peaks and troughs}$

$y = \text{displacement deviation from mean line } (\mu\text{m})$

Another surface roughness parameter is the Root Mean Square (RMS) value, which calculates the root mean square value of height deviations from the mean line [38]. Although, the Ra value is more commonly used, as a large deviation from the

average height will have less of an effect on the Ra value compared to the RMS value. A displacement outlier will therefore not skew the average roughness value.

3.5 Tensile Testing

A Zwick universal tensile tester was used to apply tensile loads to the specimens using a 10kN load cell. Forces exerted on the specimens were not expected to be higher than 5 kN [8] and therefore the 10kN load cell was assumed to be adequate while ensuring that noise did not affect the readings obtained. Wedge grips were used to grip the specimens in the tester with sandpaper folded over the gripping sections before being placed into the grips. This was to avoid slippage of the part within the grips when placed under tension, which would affect strength readings.

A crosshead speed of 2mm/min was set for all tests and crosshead displacement was measured using an extensometer. A preload of 10N was applied for each test to ensure that slack was removed from the testing rig before testing began. The test therefore only started recording data when the load cell had applied a force of 10N. This preload value was estimated to ensure that it did not interfere with the actual test data [40].

3.6 Digital Image Correlation

Digital Image Correlation (DIC) was utilized during tensile testing to measure the surface strain of each specimen at every instance of displacement. In order to perform DIC, the gauge length of each specimen was spray painted white followed by a black matte speckle pattern sprayed at random. The surface of the specimen therefore contained a highly contrasted, non-repetitive pattern so that blocks of pixels could be tracked during testing.

A camera captured grey-scale images of the speckle pattern as the specimen underwent deformation until failure. Calibration images were taken before testing to determine the imaging parameters and orientation for each specimen. A 10mm x 10mm Dantec calibration target was used for Batch 1 but for the following batches was deemed too small to calibrate the entire image correctly. A 40mm x 40mm

Dantec calibration target was thus used for Batches 2 and 3. Batches 4, 5 and 6 had already been shot with the smaller calibration target and therefore a projection file was used to calibrate their images – making the assumption that the object was perfectly planar and parallel to the camera [34]. Correlation images were then taken during deformation, after which Istra 4D was used to track the “grey value pattern” [41] to determine relative displacements within the speckle pattern. Strain values were inferred from the gradient of these displacements. [41].

3.7 Data Processing

The Zwick tensile tester outputted data of time intervals during the test and each corresponding displacement and force value. The force values were converted into engineering stress values using Equation 3 [42].

$$\sigma = \frac{F}{A} \quad [3]$$

Where $F = \text{force (N)}$

$A = \text{cross – sectional area (mm}^2\text{)}$

The cross-sectional area of each specimen was determined before testing by multiplying the width and thickness dimensions of the gauge section, as shown in Appendix A.

The displacement values obtained from the extensometer were linear as they recorded the crosshead displacement (2mm/min). These values were used to calculate engineering strain values using Equation 4 [42].

$$\varepsilon = \frac{\Delta L}{L_0} \quad [4]$$

Where $\Delta L = \text{change in length}$

$L_0 = \text{original length}$

The original gauge lengths, L_0 , were measured before testing and are shown in Appendix A.

Istra 4D was used to process the images of each speckle pattern taken during testing. Text files were outputted, which contained time steps of the test and corresponding strain values. Frames were taken every 330ms and therefore the time steps were multiplied by 0.33 in order to convert the steps into seconds. Engineering strain values were acquired by drawing a gauge length line along the ROI of the specimen within Istra 4D and obtaining strain values along that line using the 'gauge strain' feature.

Engineering stress versus strain graphs, using data obtained from the extensometer as well as DIC, were then plotted. Although, the time steps of DIC strain values and Zwick stress values were different because they were taken from the camera (set at 330ms) and testing machine, respectively. The time steps therefore needed to be matched up in order to plot graphs of these values against each other. This was performed by finding elements within each stress vector that corresponded to an element within the time vector of strain – as the strain time values were at greater intervals than the stress time values. The stress values outputted were therefore coarser than the original stress vector. Matlab performed this task as shown in Appendix C.

The Elastic Modulus, which is a measure of the stiffness of each specimen [42], was calculated within the linear elastic region of the graph using Equation 5.

$$E = \frac{\sigma}{\varepsilon} \quad [5]$$

Where $\sigma = stress (MPa)$

$\varepsilon = strain (mm/mm)$

This value was found using a best-fit line within Matlab, to determine the gradient of the linear elastic region for each stress-strain curve, as shown in Appendix C.

4. Results

4.1 Printing

4.1.1 Temperature affects on printing

Extruding and depositing ABS filament was highly affected by temperature. This was previously discussed by Tymrak et al. [7] where it was concluded that a 5°C temperature change during printing had seen to cause visible changes to the quality of a printed part.

During the investigation the extruder head and print bed were set to the required temperatures, although the ambient temperature surrounding the printer was much lower. Heat generated from the equipment rose and escaped from the printer. This caused specimens to warp as shown in Figure 21.

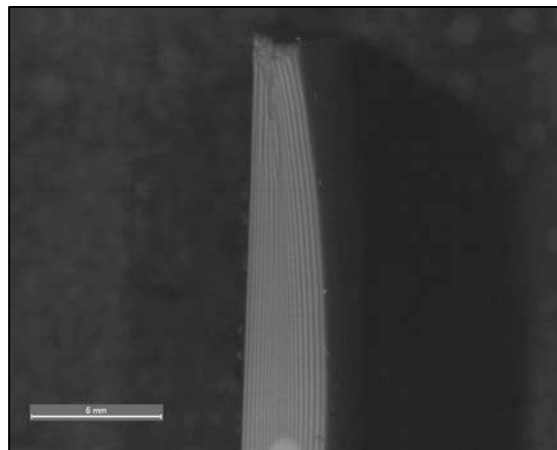


FIGURE 21: WARPING AT GRIPPING SECTION OF SPECIMEN

Warping occurred when the surface area of the initial layer did not completely adhere to the print bed but started rising at the corners of the specimen. Following deposition, the filaments at these corners contracted too quickly upon cooling due to the decreased ambient temperature and therefore detached from the print bed. Consequently, adjacent layers of filaments did not correctly deposit on top of one another with the set layer height of 0.2mm.

When the build plate adhesion type was changed from skirt to brim, which created a larger surface area of the initial layer onto the print bed – adhesion to the plate was improved and thus warping was reduced at the corners of the specimen. Although, printing a brim reduced the quality of the initial layer of the specimen– as shown in Figure 22. The quality was, however, improved through chemical post-processing.

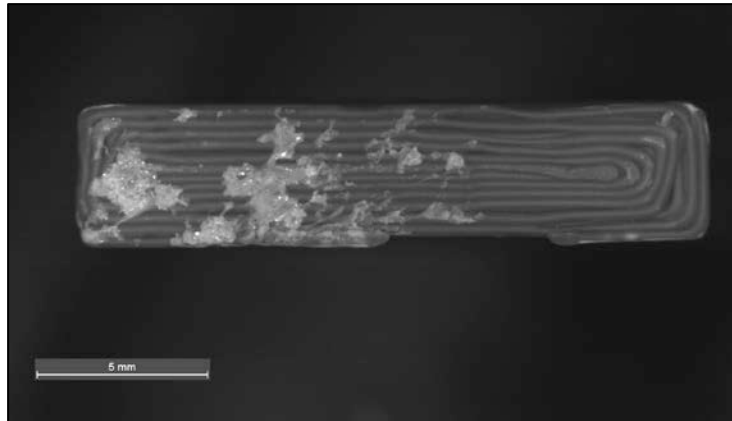


FIGURE 22: INITIAL LAYER OF UPRIGHT SPECIMEN AFTER BRIM REMOVED

In order to further reduce warping and ensure successful prints when using ABS filament – a top cover for the printer was designed that enclosed the build volume. The purpose of the top cover is to trap heat within the volume around the print bed and thus ensure that the ambient temperature is high enough to reduce shrinkage and warping. The top cover is shown in Figure 23.



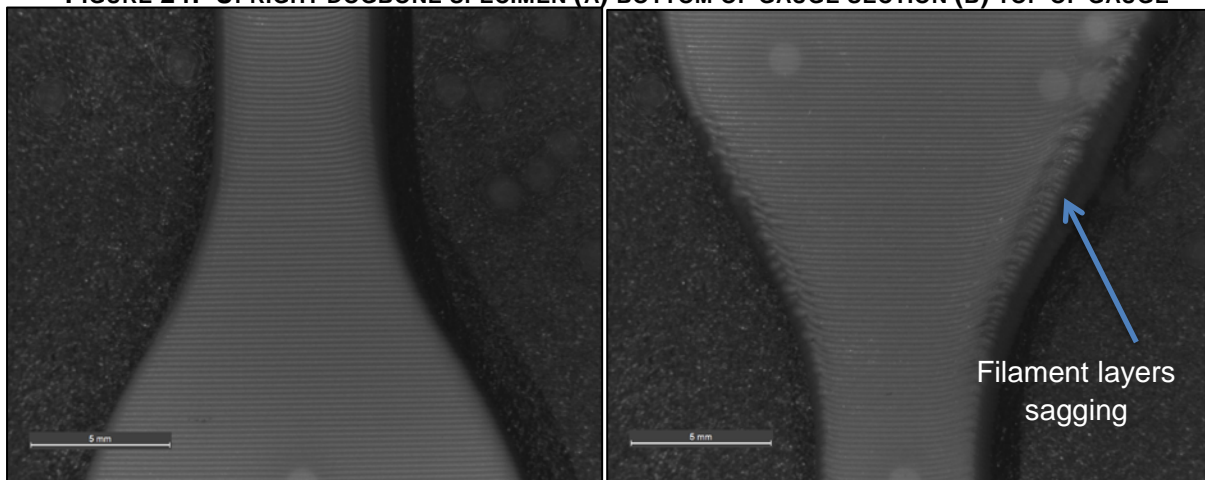
FIGURE 23: TOP COVER OF ULTIMAKER PRINTER

It was made using 5mm thick sheets of PlexiGlas (Perspex) joined together by ABS 3D-printed brackets and self-tapping screws. Although, drilling into the 3D-printed brackets was problematic if the drill piece was placed on the interface of adjacent layers, as the bracket would then split along this interface. The cover had to be high enough and extend far enough over the back of the printer to account for the filament feed roll and piping. The overhang at the back of the printer was not completely shut off as the hot air escaping would rise and therefore only the top of the cover needed to be enclosed.

4.1.2 Printing upright specimens without support material

Printing upright D638 Type IV specimens was expected to be unsuccessful because of the changing cross-sectional area of the specimen, although it was achieved without any additional support material. However, at the top of the gauge section filament layers began to slump, as they had no support of previous layers. This is shown in Figure 24 (b).

FIGURE 24: UPRIGHT DOGBONE SPECIMEN (A) BOTTOM OF GAUGE SECTION (B) TOP OF GAUGE



SECTION

This printing defect was, however, deemed acceptable within this investigation as it was not in the gauge section and was not expected to create any undesirable stress concentrations.

4.2 Chemical Post-processing

4.2.1 Microscopy Images

Images of specimens taken through a microscope, showing individual surface filaments, display the extent to which chemical exposure altered the surface of each specimen. For each microscopic area that was photographed, the left image shows the area before chemical exposure and the right image, after chemical exposure.

Figure 25 and 26 show chemical dipping and vapour smoothing of dog-bone specimens, respectively, printed in the x-direction. As can be seen, both techniques altered the surface of the part. Ridges, caused by the deposition of filaments at a 45° angle, were smoothed out through dipping. Batch 2 specimens, however, also experienced the inclusion of air bubbles into the surface of the specimen as shown in Figure 25 (a) and (b).

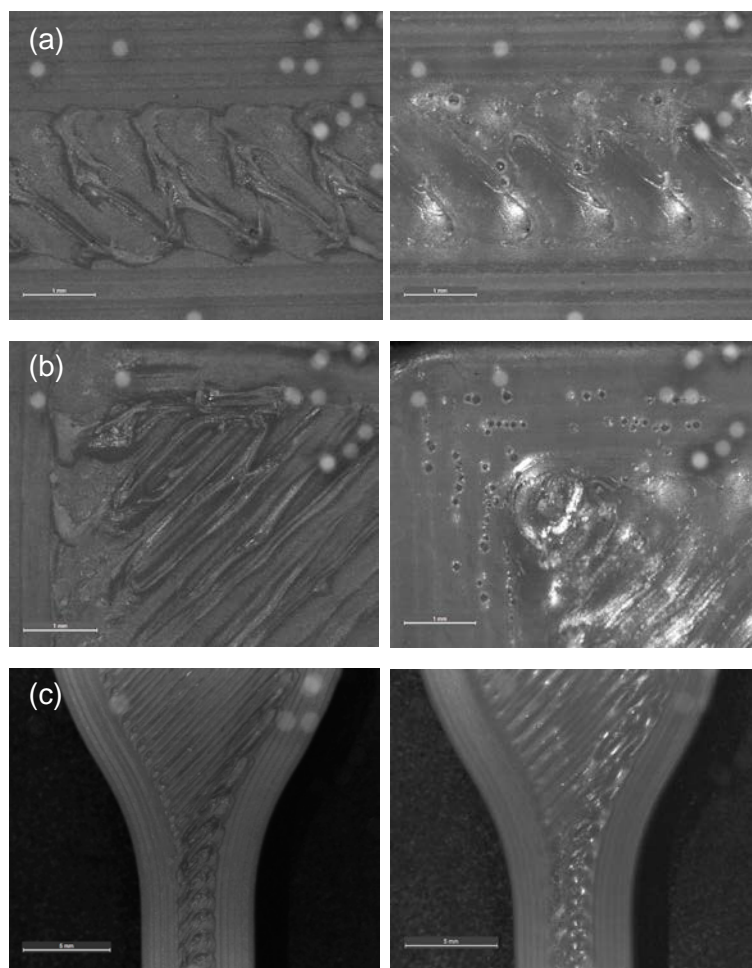


FIGURE 25: BATCH 2 (A) GAUGE SECTION (B) CORNER OF GRIPPING SECTION (C) NECK

Vapour smoothing of in-plane specimens did not have as great of an effect on the surface of each specimen compared with dipping, as surface ridges and seam lines are still clearly evident as shown in Figure 26.

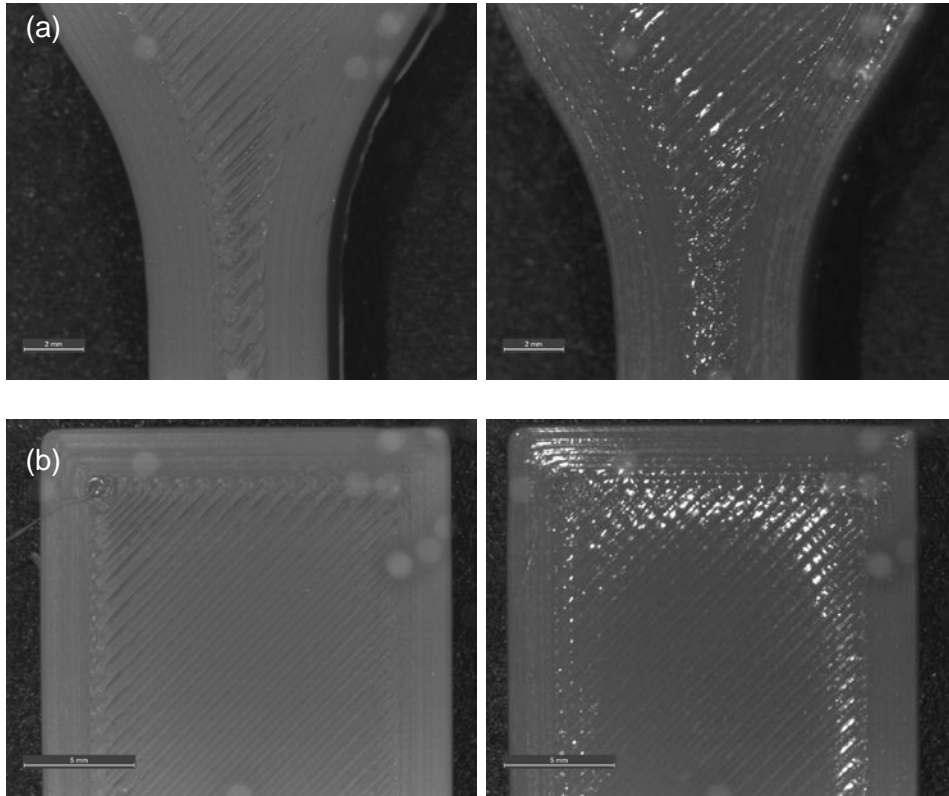


FIGURE 26: BATCH 3 (A) NECK (B) GRIPPING SECTION

Figure 27 and 28 show chemical dipping and vapour smoothing of dog-bone specimens, respectively, printed in the z-direction. Both techniques did not have a large effect on the parallel ridges of each filament layer along the surface of the specimen, which is evident in Figure 27 (a). Although bulges, whereby filaments slumped into adjacent layers at the specimen's neck, were smoothed more effectively as shown in Figure 27 (b), (c) and Figure 28.

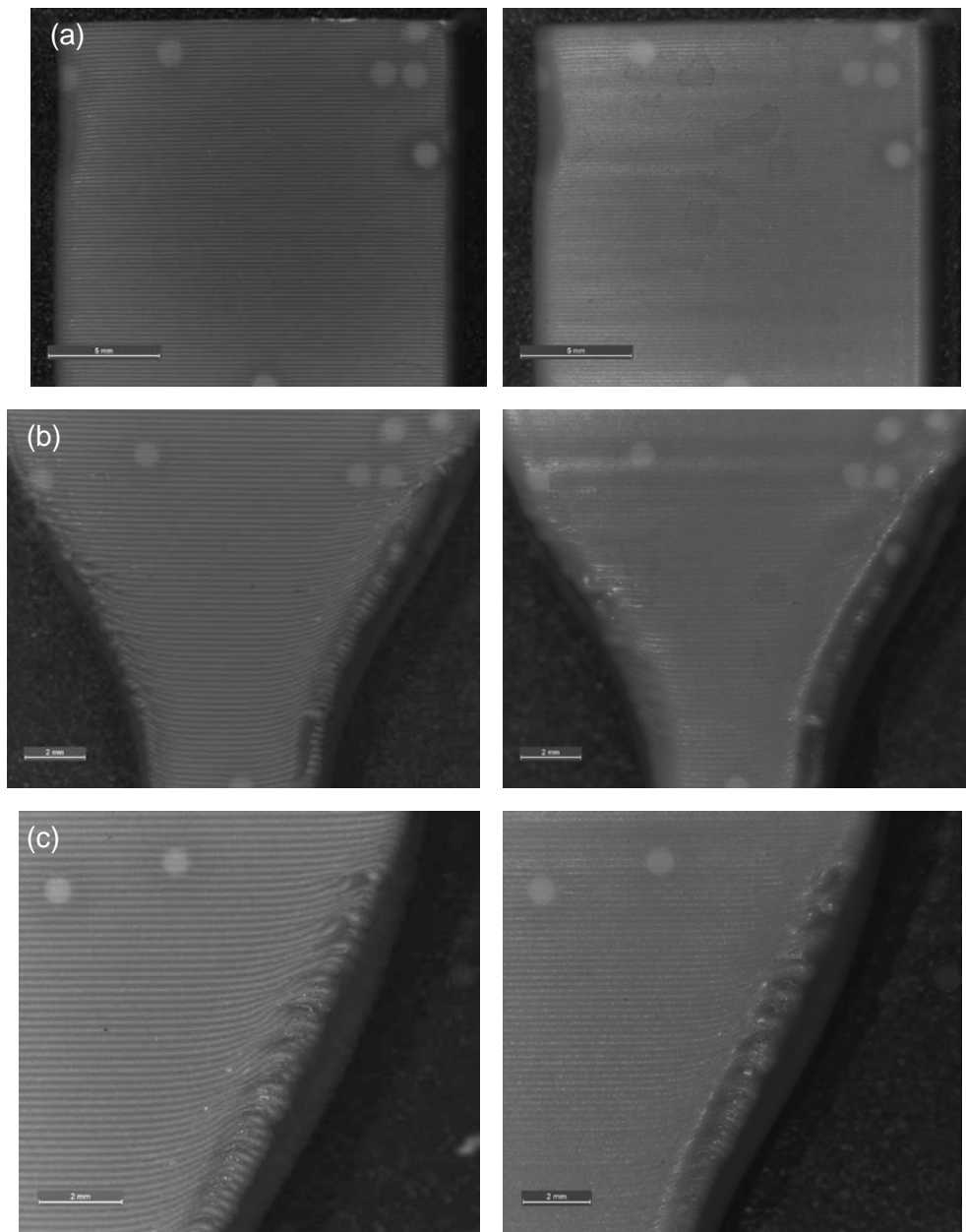


FIGURE 27: BATCH 5 (A) GRIPPING SECTION (B) NECK (C) EDGE OF GRIPPING SECTION

Both chemical treatment techniques had similar smoothing effects on each specimen. This may be attributed to the fact that upright specimens are not as conducive to smoothing by chemical exposure than in-plane specimens.

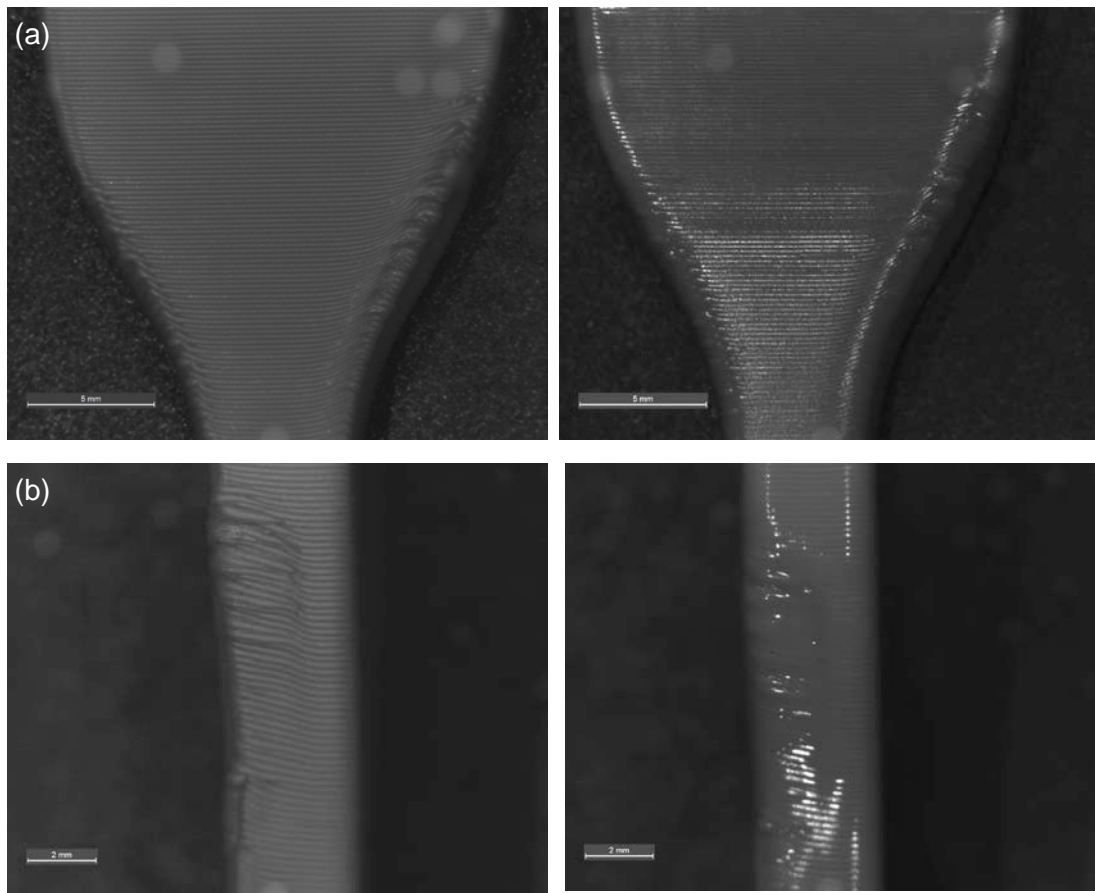


FIGURE 28: BATCH 6 (A) NECK OF SPECIMEN (B) SIDE VIEW OF NECK

In Figure 28, the seam lines between layers are still distinct after smoothing, although surfaces have a glossier finish than after dipping and filament bulges have been adequately smoothed.

4.2.2 Surface Roughness graphs

Surface roughness testing using a Profilometer produced graphs of the stylus' vertical displacement (Y) with respect to travel along each specimen's gauge length (X). The surface topography of a specimen's gauge section from each chemically post-processed batch is shown below, which depicts the average topography for that batch. Matlab was used to plot these graphs, as shown in Appendix C.

Figure 29 shows the topography of specimen 2 within Batch 2 that has been printed in the x-direction and dipped in an acetone solution.

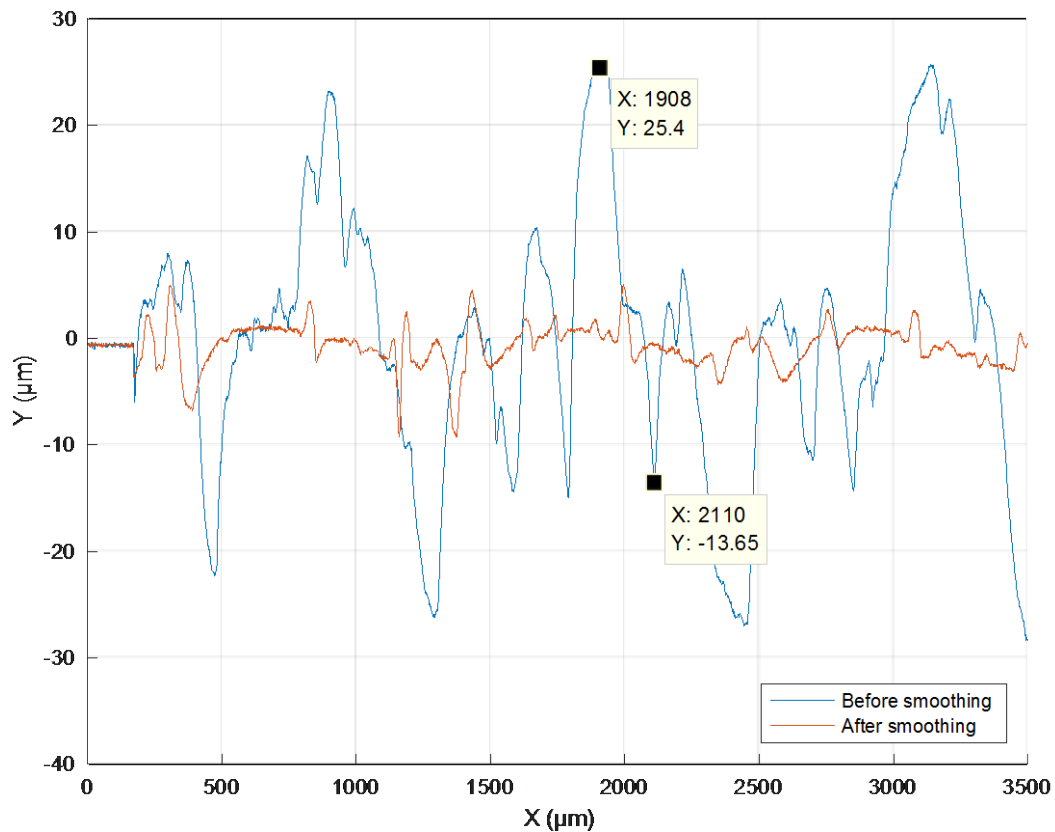


FIGURE 29: SURFACE ROUGHNESS GRAPH (BATCH 2 SPECIMEN 2)

The stylus traversed over the infill section within the gauge of each in-plane specimen – not the unidirectional perimeter lines. Filaments under the stylus therefore lay at an angle of 45° to the horizontal. The nozzle that deposited filament is 0.4mm in diameter and therefore the distance between a surface peak – where the stylus is on a filament, and a surface trough – when the stylus is between filaments, should be 0.283mm apart as shown in Equation 5.

$$\Delta X_{peak\ to\ trough} = \frac{\frac{1}{2}(0.4mm)}{\sin(45^\circ)} \quad [5]$$

$$= 0.283mm$$

The distance between a peak value and trough value shown on Figure 29, is 0.202mm. This shows that the specimen contained surface irregularities but was similar to that of theoretical values.

After dipping, the vertical displacement of peaks and troughs is reduced and the stylus motion along the X-direction is smoother as it has a larger curvature – as shown in Figure 29. The individual filaments within the gauge length are therefore not as well defined. This is also shown in Figure 25 (a).

Figure 30 shows the topography of specimen 2 within Batch 3 that has been printed in the x-direction and smoothed with acetone vapours.

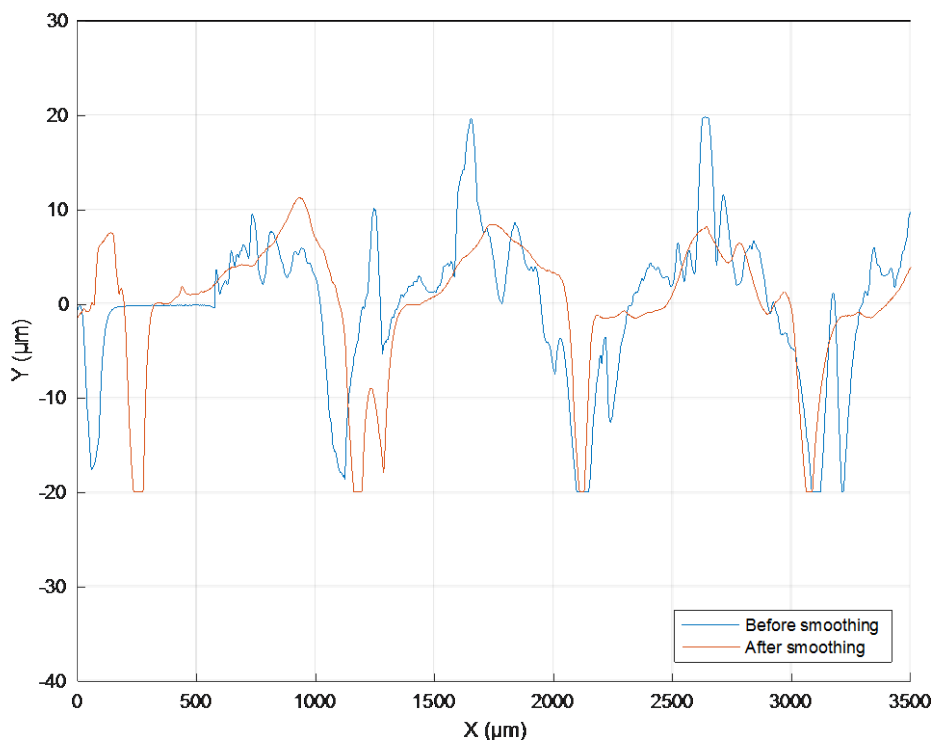


FIGURE 30: SURFACE ROUGHNESS GRAPH (BATCH 3 SPECIMEN 2)

After vapour smoothing the motion of the stylus is smoother, however the vertical displacements of the stylus have not decreased as much as for dipping of in-plane specimens. This is also shown by the evident ridges along the specimen that exist after smoothing, in Figure 26.

Figure 31 shows the topography of specimen 1 within Batch 5 that has been printed in the z-direction and dipped in an acetone solution.

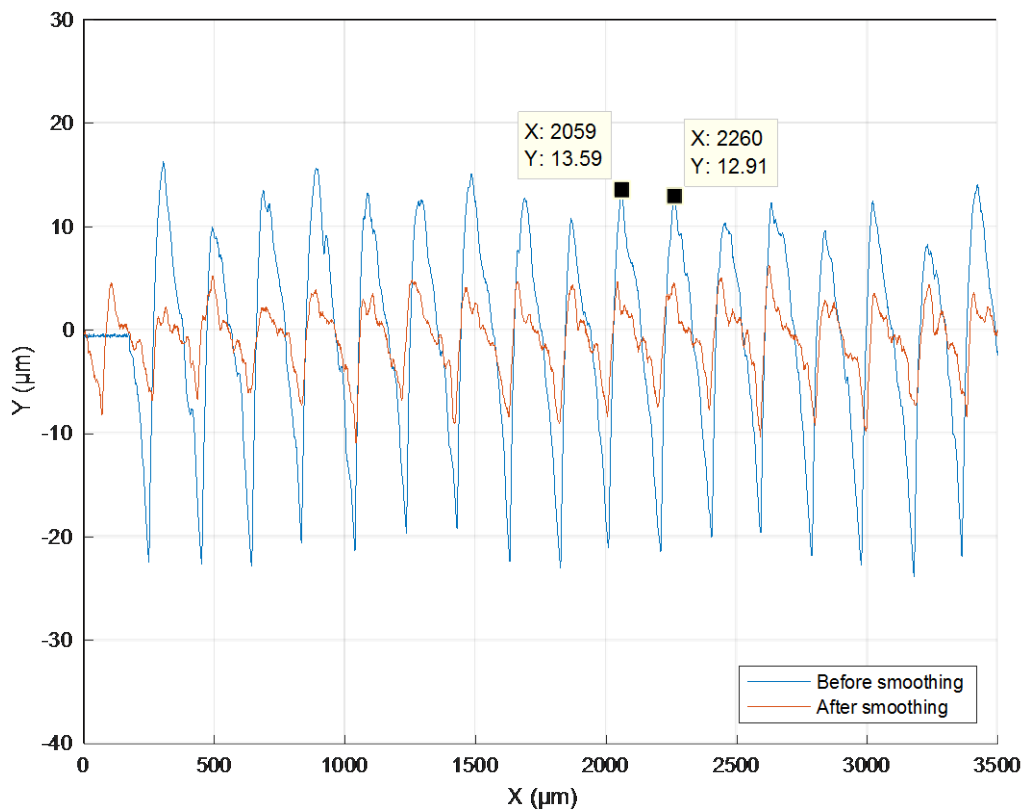


FIGURE 31: SURFACE ROUGHNESS GRAPH (BATCH 5 SPECIMEN 1)

The gauge section of interlaminar specimens consists of layers with a height of 0.2mm, lying parallel to each adjacent layer. The interval between peaks – where the stylus sits on a layer of filament, and troughs – where the stylus sits between layers, is therefore regularly spaced at 0.2mm apart. The distance between two adjacent peak values, shown in Figure 31, is 0.201mm – this shows the surface regularity of interlaminar specimens.

After dipping, the vertical displacement of the stylus has decreased but the change between displacements is still steep – unlike the increased curvature of the stylus displacement for in-plane specimens. This is also evident by seam lines still shown in Figure 27, after dipping.

Figure 32 shows the topography of specimen 1 of Batch 6 that has been printed in the z-direction and smoothed with acetone vapours.

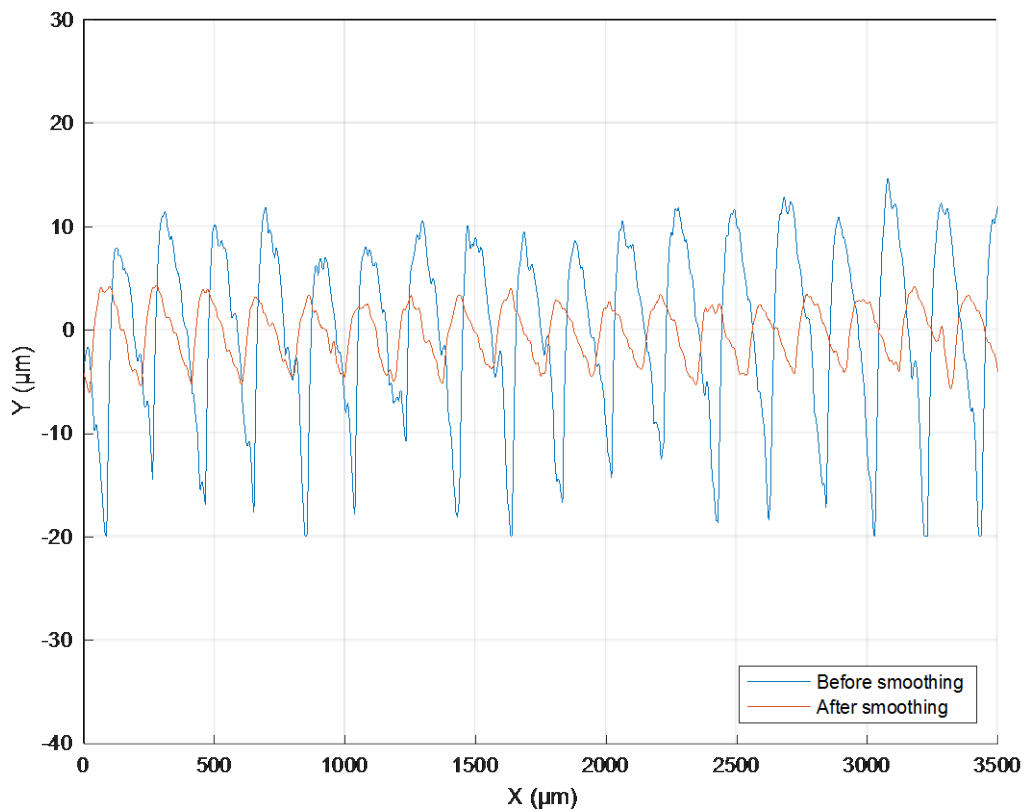


FIGURE 32: SURFACE ROUGHNESS GRAPH (BATCH 6 SPECIMEN 1)

Exposure to acetone vapours, like dipping, decreased the amplitude of peaks and troughs along the surface of the gauge length while regularity was still maintained. The plot 'after smoothing' is shifted horizontally compared with 'before smoothing', however, this is only due to the Profilometer starting at a different point along the gauge section and therefore traversing over the peaks and troughs at different stylus positions (X values).

Using the graphs produced, the maximum and minimum stylus displacements for each specimen as well as the difference between these values was found. The Ra value of the surface of each specimen was also calculated. The data within each batch was averaged and is shown in Table 3.

TABLE 3: SURFACE ROUGHNESS VALUES

	Maximum vertical displacement (μm)	Minimum vertical displacement (μm)	Difference (μm)	Ra value (μm)
In-plane specimens				
Batch 2	20.9	-28.6	49.5	6.1
Batch 2 (After dipping)	10.2	-18.8	29.1	2.4
Batch 3	17.8	-18.2	36.0	5.3
Batch 3 (After vapour smoothing)	13.0	-13.2	26.2	3.4
Interlaminar specimens				
Batch 5	14.9	-24.6	39.5	8.0
Batch 5 (After dipping)	4.7	-9.1	13.8	2.0
Batch 6	13.8	-19.9	33.7	7.8
Batch 6 (After vapour smoothing)	5.0	-6.8	11.8	2.6

4.3 Tensile testing

4.3.1 Specimen dimensions

Appendix A shows the dimensions of each specimen before tensile testing – but after chemical post-processing. Width and thickness dimensions of the gauge section were found by three measurements taken at each side and in the middle of the gauge length. A vernier caliper was used to measure these dimensions from which the cross-sectional area of the gauge was calculated. The length of the gauge was artificially produced by drawing lines on either end of the gauge and measuring this length with a ruler.

4.3.2 Strain data

An engineering strain versus time graph generated from the DIC data is shown in Figure 33. The sharp peak of the data is the point at which the specimen fractures, after which the specimen does not experience the load being applied to it anymore because it is no longer in tension. Strain therefore stops increasing after the peak point because it is no longer deforming under the applied force.

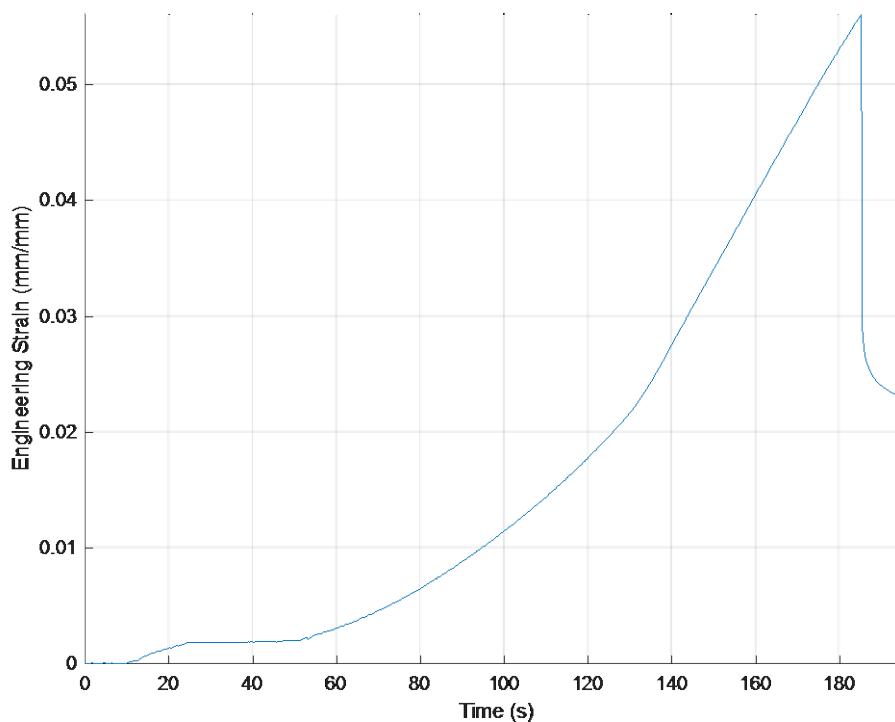


FIGURE 33: STRAIN VS. TIME GRAPH FROM DIC (BATCH 1 SPECIMEN 2)

The strain data was therefore cut at this maximum point, as any strain values after this point are not valid. At the start of the test, the specimen was not experiencing linear displacement by the crossheads and therefore a best fit line of the first linear section within the graph was used to also cut out the non-conforming initial data. The new plot using the truncated strain data is shown in Figure 34.

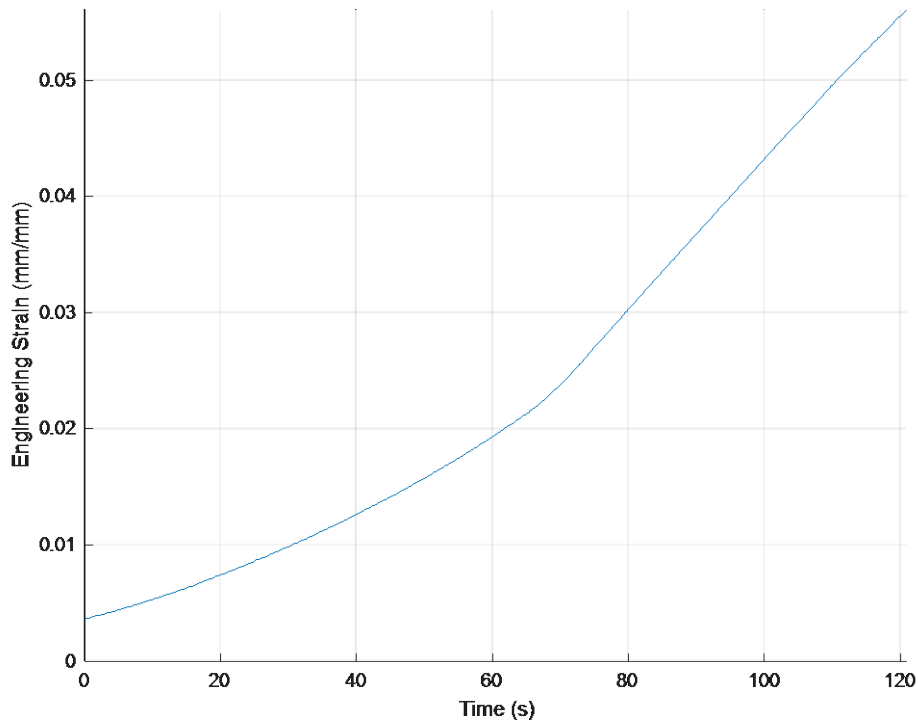


FIGURE 34: TRUNCATED STRAIN VS. TIME GRAPH (BATCH 1 SPECIMEN 2)

Although, after truncation and shifting of the graph, the time value of 0 seconds does not correspond to a strain value of 0. This is, however, acceptable because a preload of 10N was also applied to each test. The test therefore only began once slack had been taken up within the testing rig and the actual specimen had started to experience strain from the crosshead displacement.

Figure 35 shows the truncated engineering strain vs. time plot from DIC as well as the engineering strain vs. time plot from the extensometer on the same set of axis.

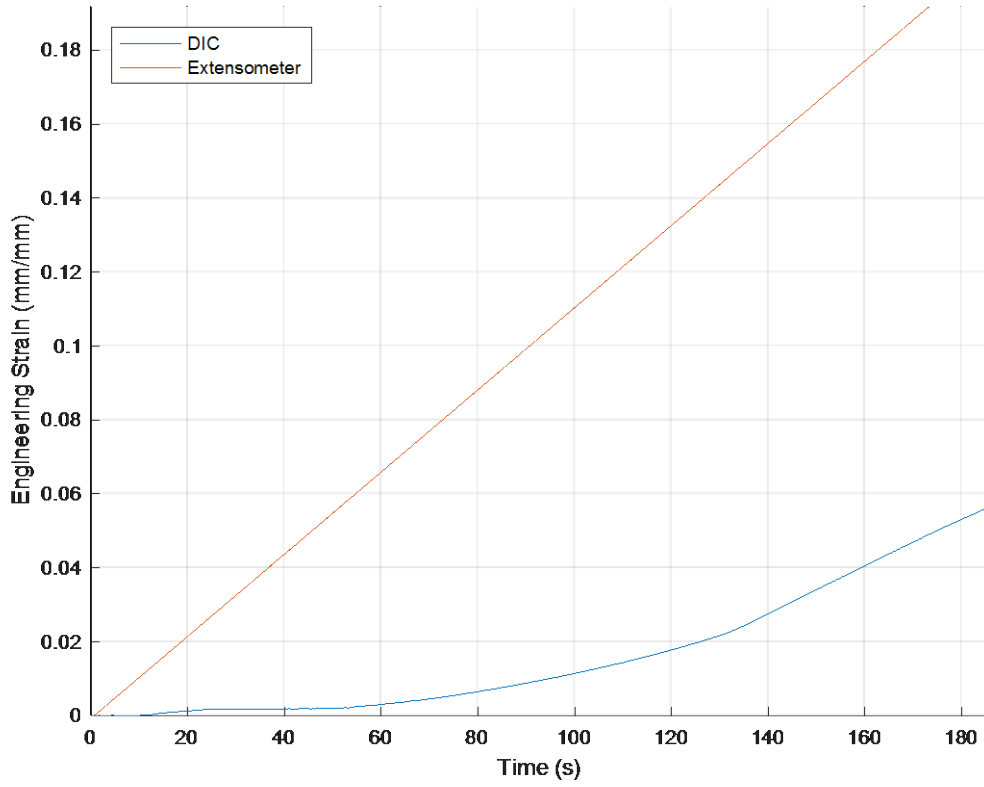


FIGURE 35: DIC AND EXTENSOMETER STRAIN VS. TIME GRAPH (BATCH 1 SPECIMEN 2)

It is evident that the strain data outputted from the extensometer is much larger than the strain data from DIC. The extensometer data is also linear as the crossheads displaced at a linear rate whereas the specimen did not experience linear strain.

4.3.3 Engineering stress vs. strain graphs

The engineering stress vs. strain graphs using extensometer data as well as DIC data for each batch is shown from Figure 36 to 47. Matlab was used to plot these graphs, as shown in Appendix C.

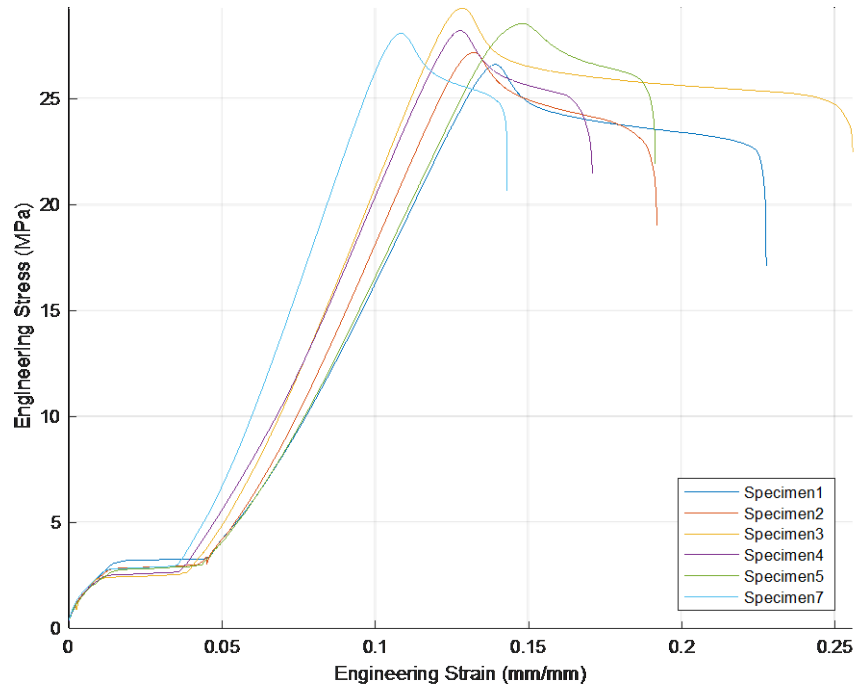


FIGURE 36: ENGINEERING STRESS VS. STRAIN FROM EXTENSOMETER (BATCH 1)

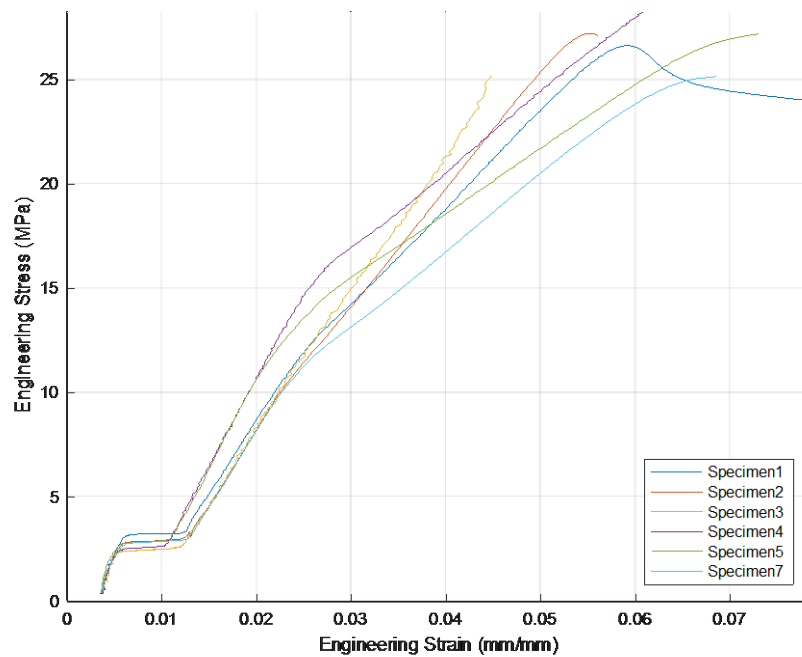


FIGURE 37: ENGINEERING STRESS VS. STRAIN FROM DIC (BATCH 1)

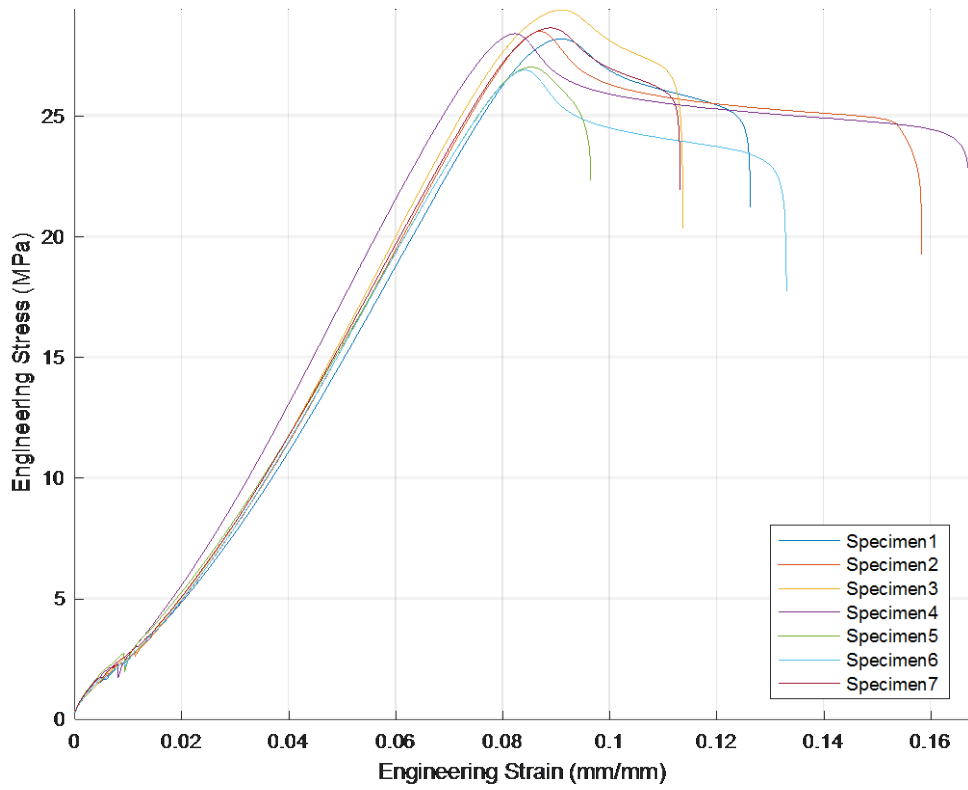


FIGURE 38: ENGINEERING STRESS VS. STRAIN FROM EXTENSOMETER (BATCH 2)

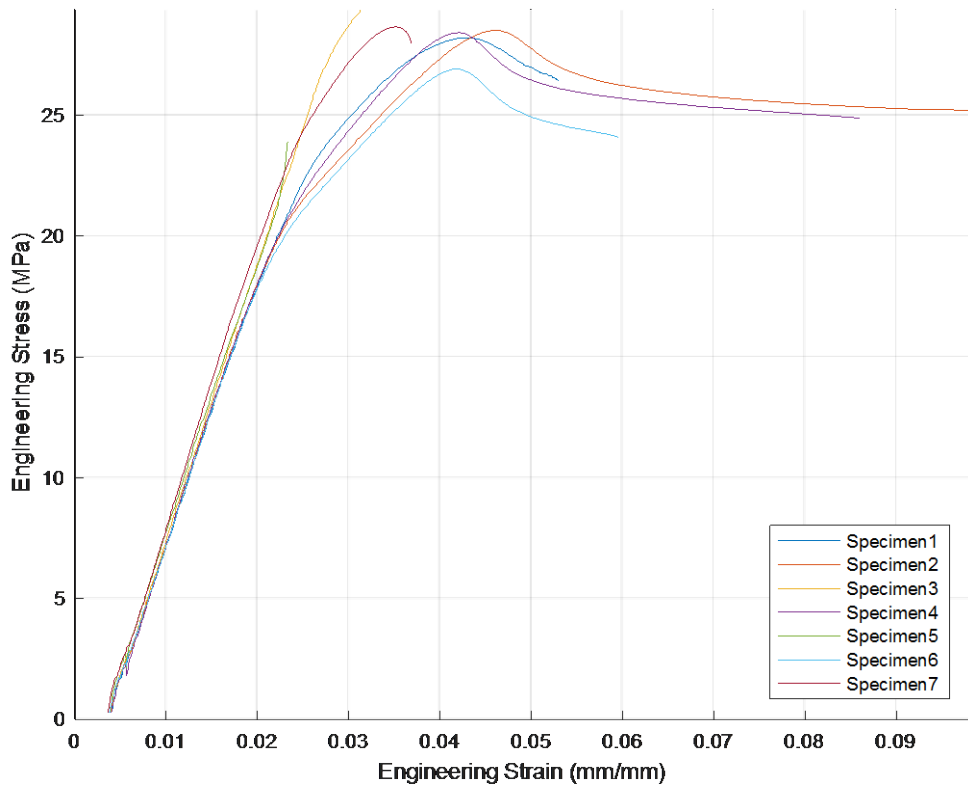


FIGURE 39: ENGINEERING STRESS VS. STRAIN FROM DIC (BATCH 2)

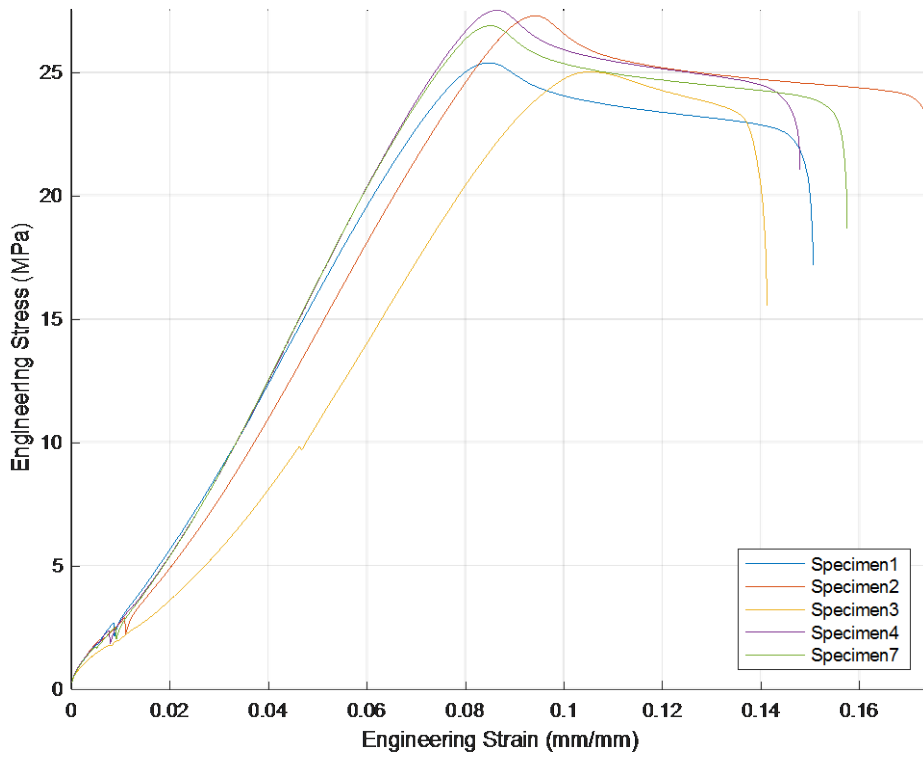


FIGURE 40: ENGINEERING STRESS VS. STRAIN FROM EXTENSOMETER (BATCH 3)

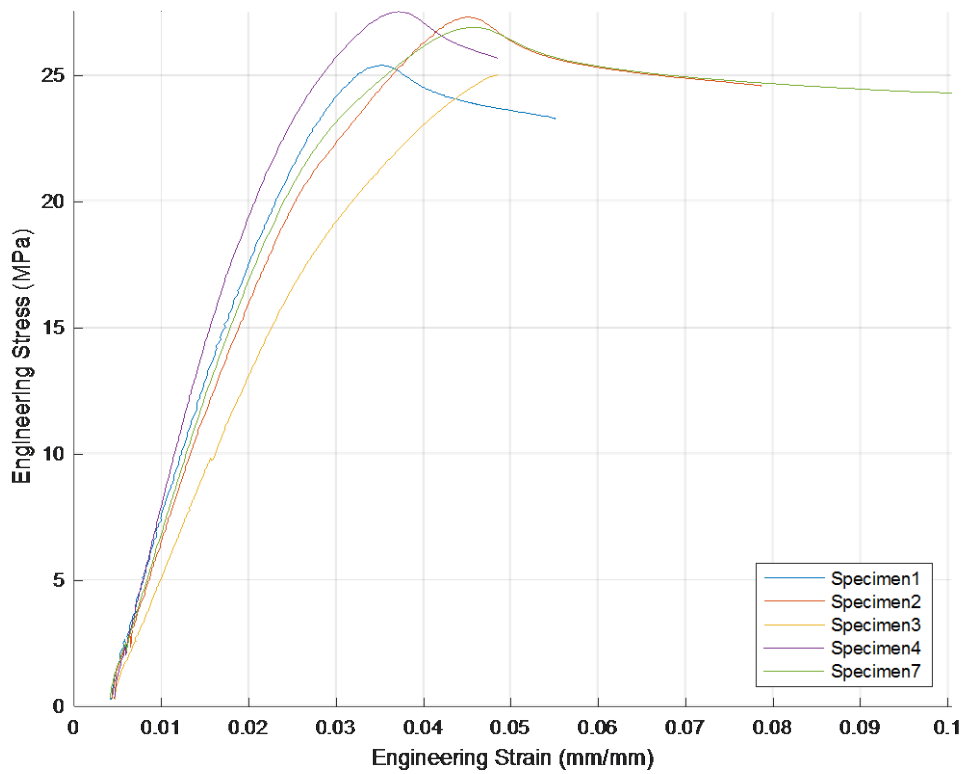


FIGURE 41: ENGINEERING STRESS VS. STRAIN FROM DIC (BATCH 3)

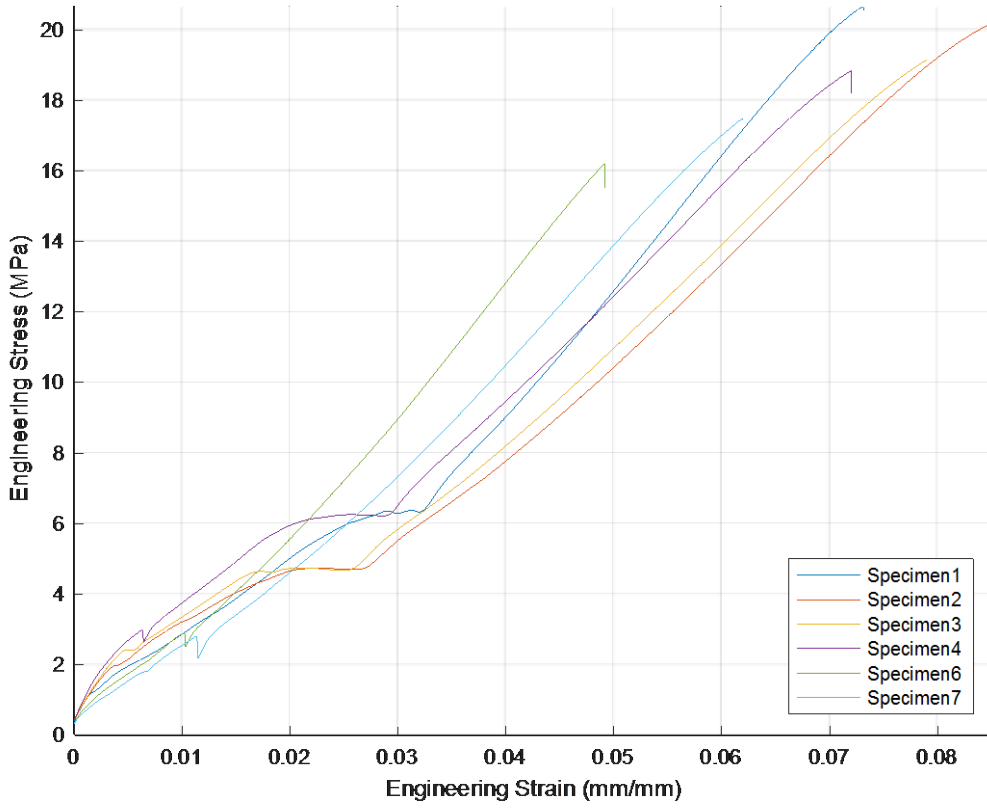


FIGURE 42: ENGINEERING STRESS VS. STRAIN FROM EXTENSOMETER (BATCH 4)

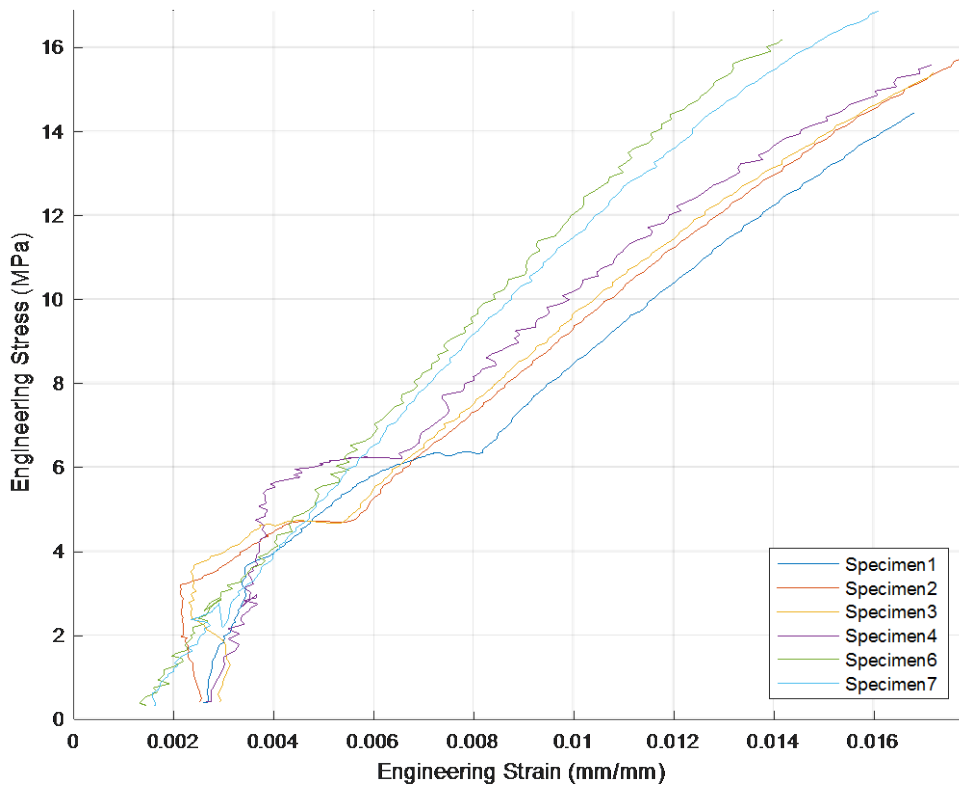


FIGURE 43: ENGINEERING STRESS VS. STRAIN FROM DIC (BATCH 4)

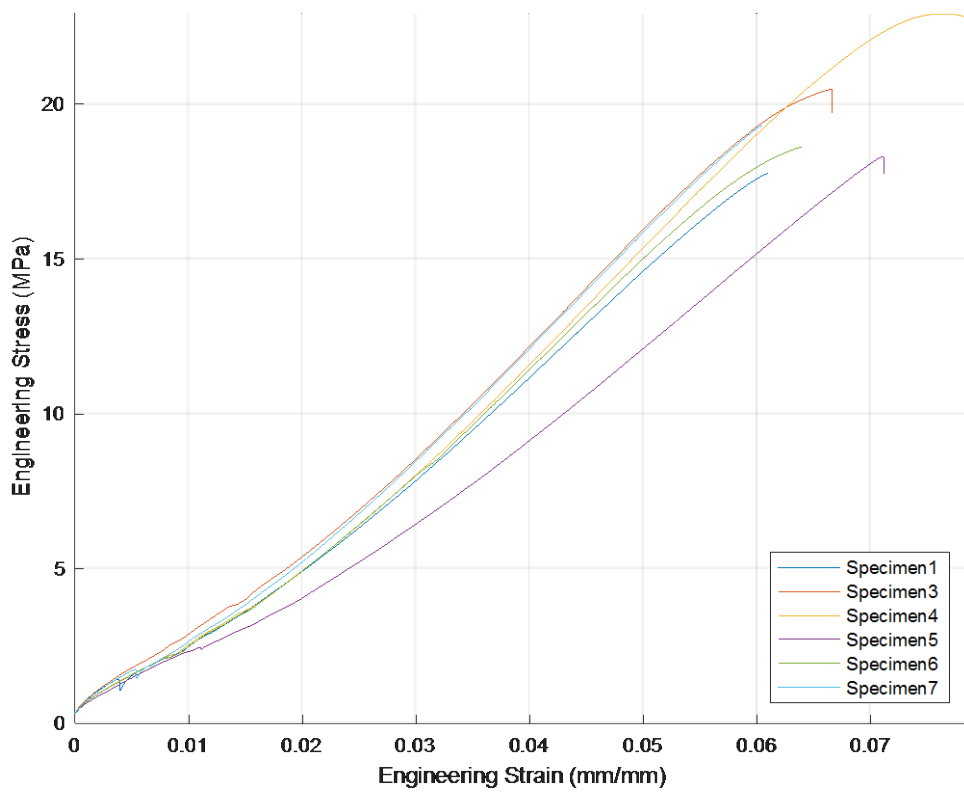


FIGURE 44: ENGINEERING STRESS VS. STRAIN FROM EXTENSOMETER (BATCH 5)

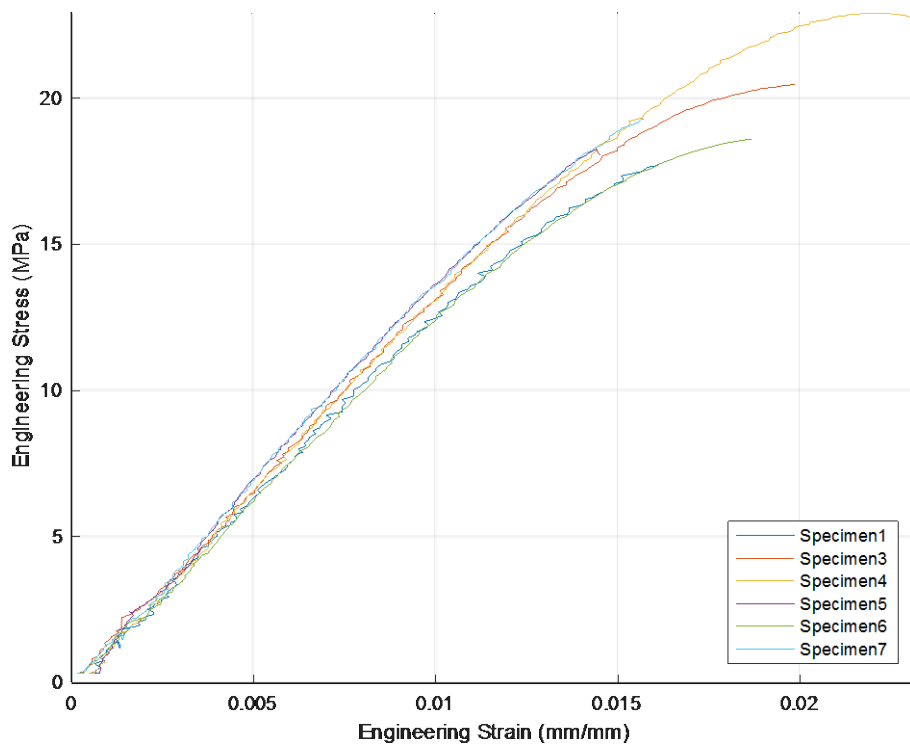


FIGURE 45: ENGINEERING STRESS VS. STRAIN FROM DIC (BATCH 5)

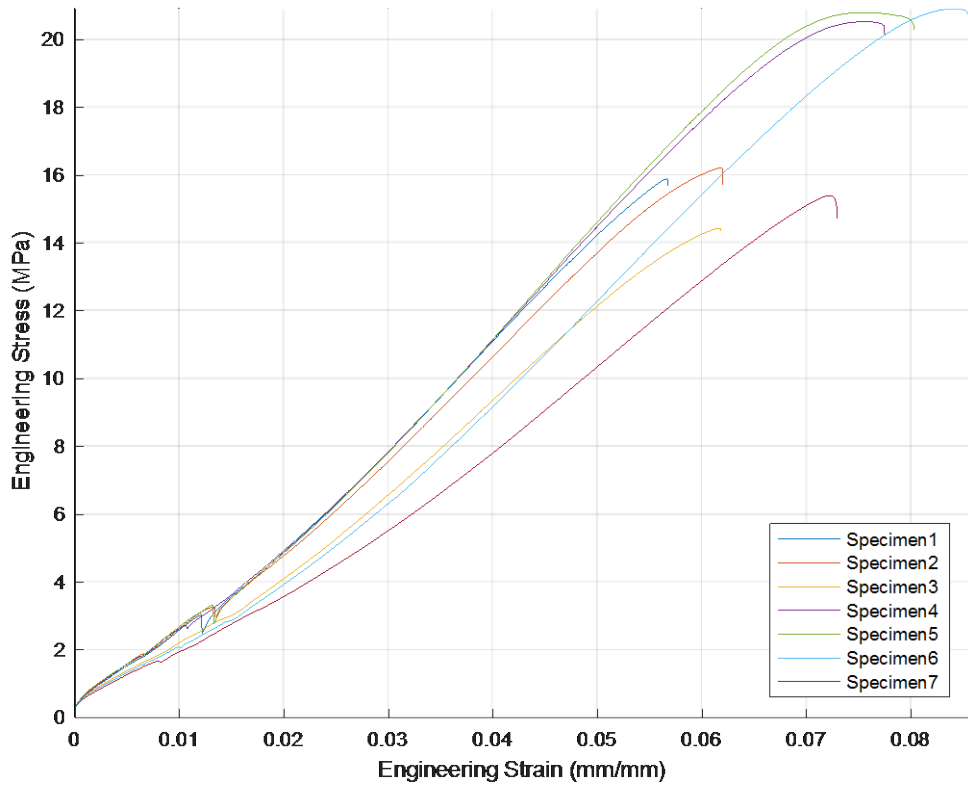


FIGURE 46: ENGINEERING STRESS VS. STRAIN FROM EXTENSOMETER (BATCH 6)

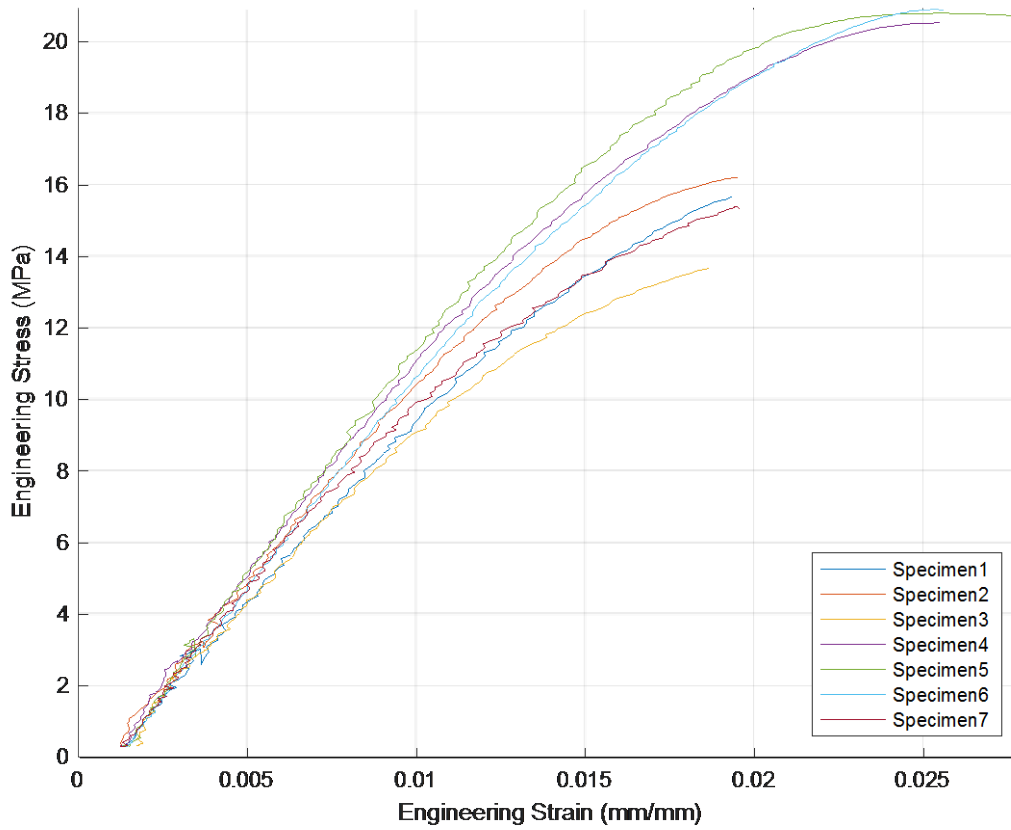


FIGURE 47: ENGINEERING STRESS VS. STRAIN FROM DIC (BATCH 6)

4.3.4 Testing errors

Five specimens from Batches 1, 3, 4 and 5 did not produce acceptable results from tensile testing and therefore are not shown on the stress vs. strain graphs. The reasons why unacceptable results were produced are stated below.

Specimen 5 in Batch 4 and specimen 2 in Batch 5 both snapped prematurely because of errors made in the tensile test program and therefore were discarded.

Specimen 6 in Batch 1 fractured at a maximum stress of 18.9MPa, which was much less than other specimens within this batch. Figure 48 also shows that the specimen snapped within its gripping section.

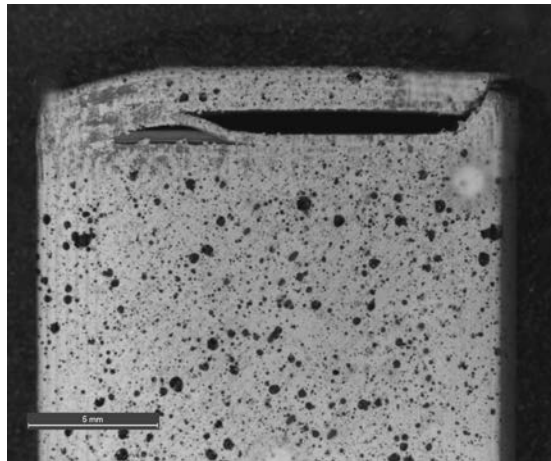


FIGURE 48: PERIMETER FRACTURE (BATCH 1 SPECIMEN 6)

Sandpaper folded over the gripping section was expected to alleviate any stress concentrations caused by damage due to the wedge grips and therefore premature failure within the gripping section was not expected. Fracturing could have, however, been due to a void within the perimeter lines, where it fractured. A void between filaments would cause a crack to initiate and propagate between the adjacent filaments and would have been created during deposition of the extruded filament onto the print bed.

Lastly, DIC processing was unable to be completed for specimens 5 and 6 within Batch 3. This was due to the specimens having a poor speckling pattern that did not achieve the specifications required to produce results from the digital photographs. The inadequate speckle pattern is shown in Figure 49.

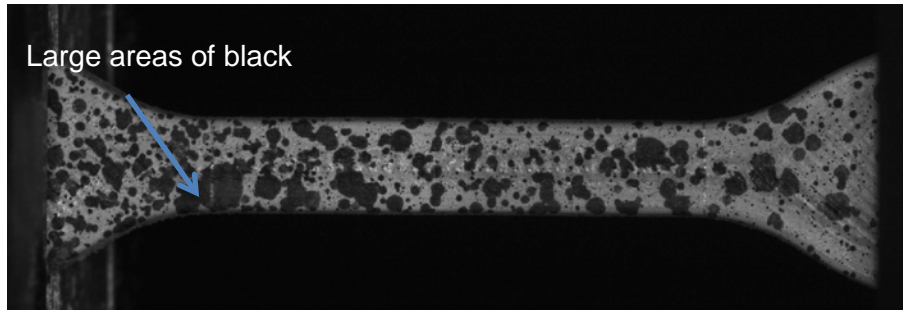


FIGURE 49: INADEQUATE SPECKLE PATTERN (BATCH 3 SPECIMEN 5)

The large areas of black spray paint on the gauge section of the specimen caused Istra 4D to not be able to distinguish the pixels as they were not well defined or highly contrasted. Strain values therefore could not be produced so that engineering stress vs. strain graphs could be plotted.

4.3.5 Data from Stress-Strain graphs

Results acquired from the engineering stress vs. strain graphs shown in Section 4.3.3; including ultimate tensile strength and strain at fracture as well as the calculated elastic moduli values are stated in Table 4.

TABLE 4: RESULTS FROM STRESS-STRAIN CURVES

	Ultimate tensile strength (MPa)		Strain at fracture (%)		Elastic Modulus (GPa)	
	Zwick	Standard deviation	Zwick	DIC	Zwick	DIC
Batch 1	28.0	0.97	19.3	6.4	0.33	0.75
Batch 2	28.2	0.90	12.9	5.5	0.40	1.11
Batch 3	26.4	1.15	15.6	6.6	0.35	0.99
Batch 4	18.8	1.67	7.1	1.7	0.31	1.10
Batch 5	19.6	1.89	6.6	2.2	0.34	1.35
Batch 6	17.7	2.87	7.2	2.2	0.30	1.13

The ultimate tensile strength as well as percentage strain at fracture of in-plane specimens is higher than that of interlaminar specimens but does not differ significantly with regards to treated or untreated specimens. The DIC strain data is much smaller than strain data from the extensometer therefore the elastic moduli calculated using DIC strains are much bigger than that of data calculated using extensometer strains. Elastic moduli values are also slightly bigger for interlaminar specimens than in-plane specimens but do not differ significantly between treated and untreated specimens.

The standard deviation of ultimate tensile strength values shows the spread of data around the mean value for each batch. It is evident that interlaminar specimens have a greater variation in data readings compared to in-plane specimens.

4.3.6 Microscopy images after fracture

The fracture faces of specimens for each batch are shown in Figure 50. Specimens printed in the x-direction can be seen by filaments running along the gauge section whereas specimens printed in the z-direction, by filaments within each layer of the gauge section. Differences between treated and untreated specimens can be seen whereby the treated in-plane specimens' faces have smaller spaces between filaments and the treated interlaminar specimens' faces are a different colour.

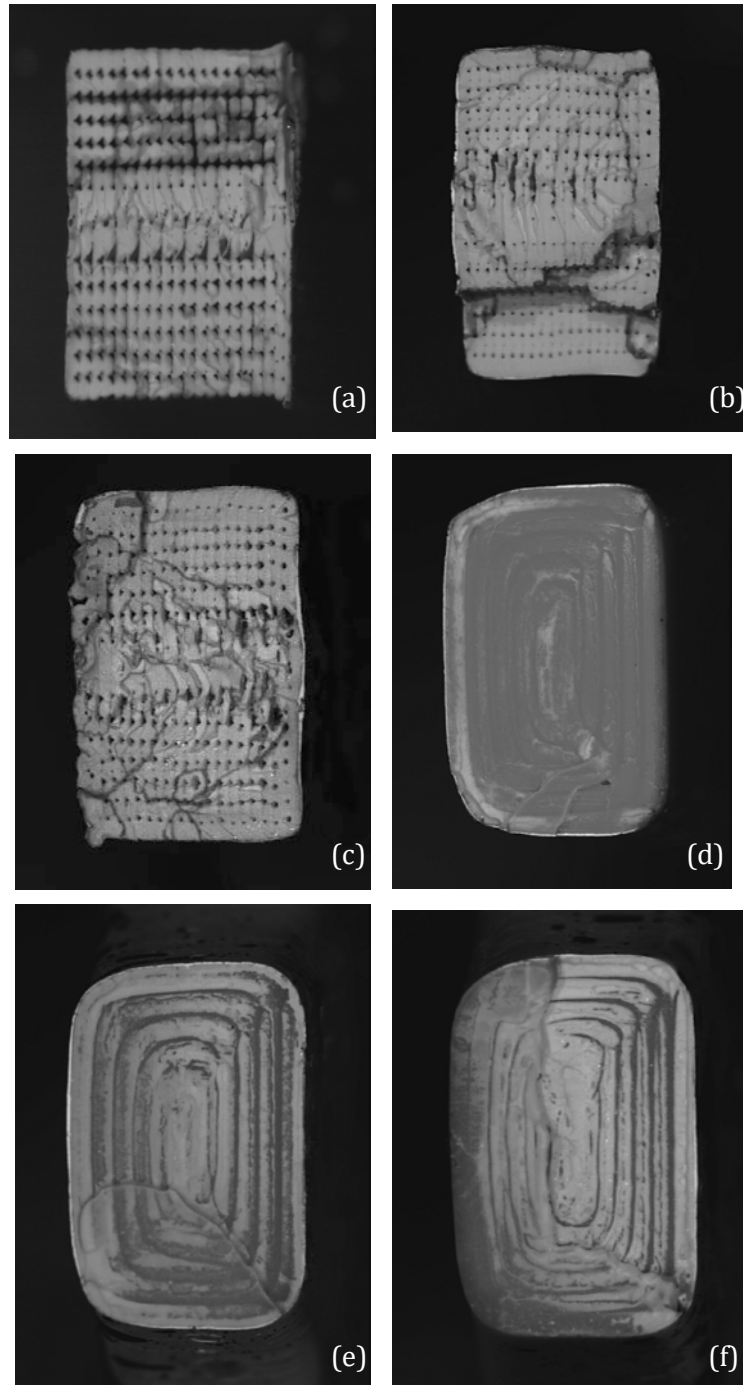


FIGURE 50: FRACTURED FACES (A) BATCH 1 (B) BATCH 2 (C) BATCH 3 (D) BATCH 4 (E) BATCH 5 (F) BATCH 6

5. Discussion

5.1 Fused Deposition Modelling using ABS filament

ABS was used as the filament material to additively manufacture specimens within this investigation, through the process of FDM. ABS was selected because it is reactive with the polar solvent acetone, as stated above, and therefore chemically treating ABS specimens will produce an effect on these specimens. ABS, however, requires a high extrusion temperature, which leads to rapid cooling of the part due to a large temperature difference between the extruded material and surrounding atmosphere. Shrinkage and part deformation thus occur if the ambient temperature is not controlled.

In order to reduce this temperature gradient, a top cover for the Ultimaker printer was made. It was effective in trapping heat inside the printer volume and therefore reducing the tendency of parts to warp. When warping is reduced; the dimensional accuracy of parts is improved, filament waste is reduced and the consistency of the printer's production is improved. Specimens printed within this investigation, before the cover was used, did not have high dimensional accuracy. Specimen dimensions, shown in Appendix A, differ from each other for the same printing parameters and surface roughness graphs show that a specimen's surface topography differs within the same batch.

If PLA was used as the filament material, the difference between the extrusion temperature and ambient temperature (without a cover) would have been smaller because PLA has a much lower glass transition temperature than ABS, 65°C compared to 105°C, and therefore has a lower extrusion temperature of 210°C. The print bed could also have been set to a lower temperature of 64°C. The reduced temperature gradient during cooling would significantly reduce the occurrences of warping of PLA specimens. However, PLA does not readily react with a common solvent and therefore chemical exposure to PLA would not have a significant effect on its filaments. The chemical treatment of parts therefore requires a compromise to be made when choosing a suitable filament material.

5.2 Chemical post-processing

Microscopy images shown in Section 4.2.1 show that specimens printed in both the x and z-directions contained surface finish defects. The stair-case and chordal effects are not evident within in-plane specimens because the faces of these specimens are only horizontal and vertical to the build plate. However, these effects can be seen at the top of the gauge section of interlaminar specimens, whereby the radii of the neck were approximated as layers of parallel filaments. When the cross-sectional area of the specimen increased, layers deposited on top of one another also started to slump onto the previous layer due to a lack of support. This further worsened the surface finish within this area. The surface of specimens within all batches also contained seam lines between deposited filaments. The poor surface quality of each specimen degraded its appearance and dimensional accuracy.

Chemical post-processing of these specimens included dipping in an acetone solution and smoothing with acetone vapours. Through chemical exposure, individual filaments softened to an extent to which the peaks of filaments filled up the troughs between filaments – this can be seen on the surface roughness graphs as the amplitude of peaks and troughs is reduced. The poor surface finish at the neck of interlaminar specimens was also smoothed to an extent – improving the dimensional accuracy of the radius, however neither method completely eradicated this deposition error.

In-plane specimens were more reactive to smoothing methods than interlaminar specimens, whereby the curvature and amplitude of surface roughness graphs was improved to a greater extent. This was in-line with the conclusion drawn by Havenga et al. [16] that horizontal specimens were smoothed to a greater extent than vertical specimens.

From the surface roughness graphs produced, it is evident that cold vapour smoothing was less effective than chemical dipping - the average roughness was reduced to a lesser extent by vapour exposure. An average Ra value for in-plane specimens improved from 6.1 μm to 2.4 μm and from 6.3 μm to 3.4 μm for dipping and vapour smoothing, respectively and for interlaminar specimens from 8.0 μm to 2.0 μm and from 7.8 μm to 2.6 μm , respectively. Although these Ra values are similar to both

values reported by Galantucci et al. [12] and Havenga et al. [16], the reduction in Ra values is smaller within this investigation. This could be attributed to the fact that specimens were exposed to acetone for shorter periods of time. During vapour smoothing, concentration levels of acetone vapours as well as the movement of vapours within the container were also not easily controlled – as shown in Appendix B.

Dipping effectively smoothed specimens in a shorter time period than vapour smoothing because dipping caused a more aggressive infiltration of acetone into the filaments of each specimen. However, if acetone vapours had been heated, greater diffusion of acetone molecules would have occurred and thus parts could have been smoothed more effectively – as shown by Havenga et al. [16]. Although, acetone at raised temperatures creates a safety risk because acetone is flammable. Vapour smoothing parts effectively and rapidly therefore requires a more complicated set-up than chemical dipping.

5.3 Tensile testing

Specimens were subjected to uniaxial tensile loads within the Zwick tensile tester, using wedge grips. The crossheads of the tester displaced at 2mm/min therefore pulling the specimen apart at a constant rate. The displacement measurements taken from the extensometer were therefore linear when plotted against the incremental time values during the test. However, displacement values from a specific point on the specimen – measured using Digital Image Correlation, produced strain results that were not linear and were much smaller than the extensometer readings. It can therefore be inferred that the specimen does not experience the constant, linear displacement of the crossheads during the entire test.

At the start of the strain versus time graph, from DIC data – as shown in Figure 33, strain values remained small and steady. Initial displacement of the crossheads was therefore not elongating the specimen but rather causing slack to be taken up within the equipment holding the grips in place – even though a preload had been applied, and causing small deformations within the grip and crosshead materials – known as machine compliance. This initial strain data was therefore removed so that only strain

experienced by the specimen was plotted. However, this truncated strain vector did not contain strain values for the entire testing time and still remained nonlinear.

The truncated strain vectors affected the engineering stress versus strain graphs that were then plotted, as the ultimate tensile strength of a specimen was not reached within every graph. This was attributed to the fact that the time vector of strain data, after truncation, which was much smaller than the time vector of stress data from the Zwick. Maximum stress values had therefore been excluded after coarser stress values were found, so that the time vectors for stress and strain were the same. This limits the accuracy of the engineering stress versus strain results obtained. However, elastic moduli obtained from the engineering stress vs. strain graphs using DIC were much closer to values within literature by Tymrak et al. [7] and Alaimo et al. [31] compared to graphs using extensometer values, which validates data obtained using DIC. Elastic moduli from the stress strain curves using extensometer readings were also much smaller than expected values, which is acceptable as strain is indirectly proportional to elastic modulus and therefore large strains will produce smaller elastic moduli.

When performing tensile tests on Batches 4, 5 and 6: a projection file was used to calibrate these tests as discussed above. The projection file assumes the specimen is completely planar and parallel to the camera – which could not practically be completely controlled. The stress strain curves of these batches are therefore assumed to be less accurate but produce acceptable results and therefore were not discarded. All stress strain curves produced from DIC are also not as smooth as graphs from the extensometer due to the coarse stress values used to plot against DIC strain. Graphs further have deviations from the linear elastic curve when plotted using DIC data, which can be attributed to strain at a specific point on the specimen momentarily stopping with an increasing stress due to a void between filaments being reached during elongation.

A standard for tension testing of 3D-printed parts has not yet been published and therefore the standard test method for tensile properties of plastics (D638) was used. This, however, assumes that the every filament will be placed in pure tension when a load is applied to it, which was not the case for FDM specimens within this

investigation – specimens contained an infill pattern whereby filaments lay at 45° to the horizontal. Data was thus expected to contain inaccuracies when using this testing method. Stress concentrations could also have been produced along the radii of the dog-bone specimens whereby filaments were deposited to approximate these radii. These filaments were not in pure tension during testing and therefore could have increased the stress state within these areas, leading to premature fracture of the part. Some specimens fractured closer to the necking region than the middle of the gauge section and therefore fracture could have been caused by the stress concentrations in this region however, the data produced during these tests was similar to tests where the specimen fractured in the centre of the gauge section and therefore tests were considered acceptable.

Standard deviations of ultimate tensile strength values for each batch, shown in Table 4, show that under the same testing parameters, the tensile results obtained from ABS specimens produced a range of values. This is especially prominent in interlaminar specimens and therefore an increased number of tests for each batch should be done to determine a more precise average. Table 4 also shows that specimens elongated along the fibre direction (in-plane) are much stronger and more ductile – larger strain values at fracture, than specimens that are elongated across layers (interlaminar).

Only the ultimate tensile strength was quoted for each specimen, as a distinct point was not visible between the elastic and plastic regions, before the ultimate tensile strength was reached. The yield strength of the material in both directions was therefore not of importance.

Specimens printed in the x-direction behaved in a ductile manner whereby a linear elastic section was followed by a plastic region, in which the ultimate tensile strength was reached, followed by fracture. However, using DIC strain values decreased the plastic region for some of the specimens. Specimens printed in the z-direction behaved in a brittle manner with no plastic region of deformation. These findings agreed with those of Song et al. [20]. Fracture faces shown in Figure 50 also show that the fracture surfaces of interlaminar specimens were perpendicular to the load applied and therefore fracturing occurred by a crack propagating between layers

whereas the fracture surfaces of in-plane specimens were not perpendicular to the load applied – some filaments within the gauge fractured before others. Fracturing therefore occurred between bonds within the filaments of these specimens.

Fracture faces further show that the chemical treatment of parts did not only affect the surface of specimens but filaments within the specimen as well. Filaments are more densely packed in in-plane specimens, after chemical exposure, therefore the ductility of the part should be increased, which was seen in research done by Galantucci et al. [8]. However, the strain at fracture was not significantly increased within Batch 2 and 3 compared with Batch 1. The fracture faces of interlaminar specimens are also discoloured after chemical exposure and therefore it could be expected that chemical exposure caused an increased bond between layers due to the melting of filaments. However, the strain at fracture was not significantly increased for Batches 5 and 6, either. The chemical treatment of specimens therefore did not affect their microscopic mechanical properties of ductility and strength.

More accurate stress versus strain graphs could have been produced using true stress and true strain values. True stress accounts for the changing cross-sectional area of the specimen during deformation in order to calculate stress. This was not measured within this investigation, as determining the change in cross-sectional area was difficult as DIC was only performed in one plane. However if true stress was calculated, true strain could also be calculated – whereby the changing length of the specimen during elongation is accounted for, using DIC due to its accuracy in measuring strain of the specimen.

6. Conclusion and Recommendations

Within this project, ABS specimens were printed through the method of FDM and effectively smoothed using the chemical treatment methods of dipping and vapour smoothing. In-plane as well as interlaminar tensile testing showed that chemical exposure to FDM specimens did not have a significant effect on their strength or ductility, however tensile properties were greatly affected by a specimen's filament orientation in relation to the pull direction during tensile testing.

Both dipping in an acetone solution as well as exposure to acetone vapours improved the appearance of ABS parts as their surfaces were smoothed – producing a glossy surface finish. Microscopic peaks and valleys on a part's surface, created by deposited filaments, were flattened and the average roughness value for each specimen was reduced through chemical exposure. However, seam lines and ridges along each specimen's surface still remained and therefore chemical exposure did not completely eradicate the surface defects attributed to FDM.

Results obtained from tensile tests showed that in-plane specimens have superior tensile properties compared with interlaminar specimens as they can withstand much higher stresses and undergo greater elongation before fracturing. In-plane specimens behaved in a ductile manner whereas interlaminar specimens behaved in a brittle manner. Using two methods to determine strain during tensile tests – an extensometer and DIC, showed that the specimen undergoing deformation did not experience the linear displacement of the crossheads throughout the experiment and therefore the non-contact method of DIC produced more accurate results compared with the extensometer readings.

This investigation was therefore successful in determining the extent to which chemical post-processing affects the tensile properties of FDM parts as chemical exposure to ABS specimens improved their surface finish without significantly altering their tensile properties or strength capabilities. The results obtained provide improved design guidelines and material properties regarding the surface finish and strength of ABS specimens for designers using 3D printers.

Limitations of this investigation include the fact that only ABS as a filament material can be produced through FDM and then effectively smoothed using a chemical solvent and only two techniques regarding chemical smoothing of parts were investigated. The in-plane and interlaminar pull directions were also the only pull directions investigated when regarding the anisotropic nature of FDM parts.

Recommendations to improve the results obtained within this investigation include; using true stress versus true strain data so that the changing cross-sectional area and gauge length during elongation are accounted for, optimising the concentration and immersion time of chemical treatments so that specimens are smoothed with greater precision and to a larger extent, improving the tensile testing standard geometry for FDM parts to reduce stress concentrations, improving printing methods of ABS to reduce temperature effects and increasing the number of tests conducted for each batch so that more accurate and precise tensile properties can be found.

References

- [1] ASTM International. ASTM ISO/ASTM52900-15 Standard Terminology for Additive Manufacturing – General Principles – Terminology. West Conshohocken, PA: ASTM International, 2015. Available at: <https://doi-org.ezproxy.uct.ac.za/10.1520/ISOASTM52900-15>.
- [2] B. Berman, "3-D printing: The new industrial revolution," *Business Horizons*, vol. 55, no. 2, pp. 155-162, 2012.
- [3] E. M. Sachs, J. S. Haggerty, M. J. Cima, and P. A. Williams, "Three-dimensional printing techniques," ed: Google Patents, 1993.
- [4] N. Hopkinson, R. Hague, and P. Dickens, *Rapid Manufacturing: An Industrial Revolution for the Digital Age*. Wiley, 2006.
- [5] S. S. Crump, "Apparatus and method for creating three-dimensional objects," ed: Google Patents, 1992.
- [6] J. M. Chacón, M. A. Caminero, E. García-Plaza, and P. J. Núñez, "Additive manufacturing of PLA structures using fused deposition modelling: Effect of process parameters on mechanical properties and their optimal selection," *Materials & Design*, vol. 124, pp. 143-157, 2017.
- [7] B. M. Tymrak, M. Kreiger, and J. M. Pearce, "Mechanical properties of components fabricated with open-source 3-D printers under realistic environmental conditions," *Materials & Design*, vol. 58, pp. 242-246, 2014.
- [8] L. M. Galantucci, F. Lavecchia, and G. Percoco, "Quantitative analysis of a chemical treatment to reduce roughness of parts fabricated using fused deposition modeling," *CIRP Annals - Manufacturing Technology*, vol. 59, no. 1, pp. 247-250, 2010.
- [9] X. Wang, M. Jiang, Z. Zhou, J. Gou, and D. Hui, "3D printing of polymer matrix composites: A review and prospective," *Composites Part B: Engineering*, vol. 110, pp. 442-458, 2017.
- [10] M. K. Agarwala, V. R. Jamalabad, N. A. Langrana, A. Safari, P. J. Whalen, and S. C. Danforth, "Structural quality of parts processed by fused deposition," *Rapid Prototyping Journal*, vol. 2, no. 4, pp. 4-19, 1996.
- [11] X. Yan and P. Gu, "A review of rapid prototyping technologies and systems," *Computer-Aided Design*, vol. 28, no. 4, pp. 307-318, 1996/04/01/ 1996.

- [12] L. M. Galantucci, F. Lavecchia, and G. Percoco, "Experimental study aiming to enhance the surface finish of fused deposition modeled parts," *CIRP Annals - Manufacturing Technology*, vol. 58, no. 1, pp. 189-192, 2009.
- [13] P.-T. Lan, S.-Y. Chou, L.-L. Chen, and D. Gemmill, "Determining fabrication orientations for rapid prototyping with Stereolithography apparatus," *Computer-Aided Design*, vol. 29, no. 1, pp. 53-62, 1997/01/01/ 1997.
- [14] P. M. Pandey, N. Venkata Reddy, and S. G. Dhande, "Improvement of surface finish by staircase machining in fused deposition modeling," *Journal of Materials Processing Technology*, vol. 132, no. 1, pp. 323-331, 2003/01/10/ 2003.
- [15] Y. Jin, Y. Wan, B. Zhang, and Z. Liu, "Modeling of the chemical finishing process for polylactic acid parts in fused deposition modeling and investigation of its tensile properties," *Journal of Materials Processing Technology*, vol. 240, pp. 233-239, 2017.
- [16] S.P. Havenga, D.J. De Beer, P.J. Van Tonder, R.I. Campbell. (2015). "Effectiveness of acetone post-production finishing on entry-level FDM-printed ABS artefacts", in *Proc. of RAPDASA, 2015, Pretoria* [Online]. Available at:
https://www.researchgate.net/publication/305392116_Effectiveness_of_acetone_post-production_finishing_on_entry-level_FDM-printed_ABS_artefacts
- [17] R. L. Zinniel, "Vapor smoothing surface finishing system," ed: Google Patents, 2011.
- [18] R. Singh, S. Singh, I. P. Singh, F. Fabbrocino, and F. Fraternali, "Investigation for surface finish improvement of FDM parts by vapor smoothing process," *Composites Part B: Engineering*, vol. 111, pp. 228-234, 2017.
- [19] J. S. Chohan, R. Singh, K. S. Boparai, R. Penna, and F. Fraternali, "Dimensional accuracy analysis of coupled fused deposition modeling and vapour smoothing operations for biomedical applications," *Composites Part B: Engineering*, vol. 117, pp. 138-149, 2017.
- [20] Y. Song, Y. Li, W. Song, K. Yee, K. Y. Lee, and V. L. Tagarielli, "Measurements of the mechanical response of unidirectional 3D-printed PLA," *Materials & Design*, vol. 123, pp. 154-164, 2017.

- [21] NA. (2016). "Validating isotropy in SLA 3D printing." Available at: <https://formlabs.com/blog/isotropy-in-SLA-3D-printing/>
- [22] A. K. Sood, R. K. Ohdar, and S. S. Mahapatra, "Parametric appraisal of mechanical property of fused deposition modelling processed parts," *Materials & Design*, vol. 31, no. 1, pp. 287-295, 2010.
- [23] J. Cantrell *et al.*, "Experimental Characterization of the Mechanical Properties of 3D Printed ABS and Polycarbonate Parts," in *Advancement of Optical Methods in Experimental Mechanics, Volume 3: Proceedings of the 2016 Annual Conference on Experimental and Applied Mechanics* S. Yoshida, L. Lamberti, and C. Sciammarella, Eds. Cham: Springer International Publishing, 2017, pp. 89-105.
- [24] ASTM D638-14 Standard Test Method for Tensile Properties of Plastics, ASTM International, West Conshohocken, PA, 2014, <https://doi-org.ezproxy.uct.ac.za/10.1520/D0638-14>
- [25] ASTM D3039/D3039M-14 Standard Test Method for Tensile Properties of Polymer Matrix Composite Materials, ASTM International, West Conshohocken, PA, 2014, https://doi-org.ezproxy.uct.ac.za/10.1520/D3039_D3039M-14
- [26] J. F. Rodríguez, J. P. Thomas, and J. E. Renaud, "Mechanical behavior of acrylonitrile butadiene styrene (ABS) fused deposition materials. Experimental investigation," *Rapid Prototyping Journal*, vol. 7, no. 3, pp. 148-158, 2001.
- [27] NA. (2016). "RepRap ABS". Available at: <http://reprap.org/wiki/ABS>
- [28] Bagsik, A. (2011). "Mechanical properties of Fused Deposition Modeling Parts Manufactured with ULTEM*9085." Available at: <http://usglobalimages.stratasys.com/Main/Files/FDM%20Test%20Reports/Mechanical%20Properties%20of%20Ultem%20FDM%20Parts.pdf?v=634600740965345576>
- [29] D. Adams. (2011). "Tabbing composite test specimens: When and why." Available at: <http://www.compositesworld.com/articles/tabbing-composite-test-specimens-when-and-why>

- [30] C. Yang, X. Tian, D. Li, Y. Cao, F. Zhao, and C. Shi, "Influence of thermal processing conditions in 3D printing on the crystallinity and mechanical properties of PEEK material," *Journal of Materials Processing Technology*, vol. 248, pp. 1-7, 10// 2017.
- [31] G. Alaimo, S. Marconi, L. Costato, and F. Auricchio, "Influence of meso-structure and chemical composition on FDM 3D-printed parts," *Composites Part B: Engineering*, vol. 113, no. Supplement C, pp. 371-380, 2017/03/15/ 2017.
- [32] N. McCormick and J. Lord, "Digital Image Correlation," *Materials Today*, vol. 13, no. 12, pp. 52-54, 2010/12/01/ 2010.
- [33] S. Lin, "Strain Measurement using Digital Image Correlation", Royal Institute of Technology, Sweden, 2015.
- [34] Correlated Solutions Inc., "Digital Image Correlation: Overview of Principles and Software", University of South Carolina, 2009.
- [35] "Platform adhesion settings in Cura. | Ultimaker", *Ultimaker.com*, 2017. [Online]. Available: <https://ultimaker.com/en/resources/20423-platform-adhesion-cura>.
- [36] "Polypropylene PP - Chemical Resistance", *Engineeringtoolbox.com*, 2017. [Online]. Available: https://www.engineeringtoolbox.com/polypropylene-pp-chemical-resistance-d_435.html.
- [37] "Profilometer", *En.wikipedia.org*, 2017. [Online]. Available: <https://en.wikipedia.org/wiki/Profilometer>.
- [38] H. L.P., "Ra & RMS Surface Roughness Calculation - Surface Finish Formulas | Harrison Electropolishing L.P.", *Harrisonep.com*, 2017. [Online]. Available: <http://www.harrisonep.com/electropolishing-ra.html>.
- [39] "Surface roughness", *En.wikipedia.org*, 2017. [Online]. Available: https://en.wikipedia.org/wiki/Surface_roughness.
- [40] "Preloading, and How It Affects Your Mechanical Test - Instron", *Instron.us*, 2017. [Online]. Available: <http://www.instron.us/en-us/our-company/press-room/blog/2014/august/preloading-and-how-it-affects-your-mechanical-test>.

- [41] "Digital Image Correlation (DIC) Measurement Principles", *Dantecdynamics.com*, 2017. [Online]. Available: <https://www.dantecdynamics.com/measurement-principles-of-dic>.
- [42] "Modulus of Elasticity or Young's Modulus - and Tensile Modulus for common Materials", *Engineeringtoolbox.com*, 2017. [Online]. Available: https://www.engineeringtoolbox.com/young-modulus-d_417.html.

Appendix A: Specimen dimensions

	Overall length (mm)	Gauge length (mm)	Width (mm)	Thickness (mm)	Cross-sectional area (mm ²)
Batch 1					
Specimen 1	114.3	30	6.2	4.1	25.4
Specimen 2	114.5	30	6.4	4.0	25.6
Specimen 3	114.3	30	6.1	4.1	24.7
Specimen 4	114.4	35	6.3	4.2	26.3
Specimen 5	144.0	33	6.3	4.0	25.2
Specimen 6	114.3	33	6.1	4.2	25.3
Specimen 7	114.4	35	6.2	4.0	24.7
Batch 2					
Specimen 1	114.1	33	6.5	4.1	26.5
Specimen 2	114.1	33	6.5	4.2	27.4
Specimen 3	114.4	33	6.1	4.1	25.1
Specimen 4	114.3	32	6.2	4.2	26.0
Specimen 5	114.4	34	6.5	4.4	28.4
Specimen 6	114.2	33	6.6	4.4	29.1
Specimen 7	114.5	32	6.3	4.2	26.5
Batch 3					
Specimen 1	114.0	33	6.4	4.3	27.9
Specimen 2	114.5	30	6.4	4.3	27.5
Specimen 3	114.0	32	6.0	4.1	24.9
Specimen 4	114.3	32	6.3	4.2	26.7
Specimen 5	114.4	33	6.4	4.3	27.9
Specimen 6	114.5	32	6.5	4.3	28.2
Specimen 7	114.4	31	6.4	4.3	27.3
Batch 4					

Specimen 1	114.2	37	6.1	4.2	25.8
Specimen 2	114.5	32	6.1	4.1	25.2
Specimen 3	114.4	32	6.1	4.1	24.9
Specimen 4	114.5	34	6.1	4.1	24.9
Specimen 5	114.4	33	6.1	4.1	25.1
Specimen 6	114.4	32	6.1	4.1	25.0
Specimen 7	114.4	33	6.1	4.1	25.1
Batch 5					
Specimen 1	114.6	35	6.2	4.1	25.6
Specimen 2	114.7	34	6.0	4.2	25.2
Specimen 3	114.6	35	6.1	4.2	25.8
Specimen 4	114.5	34	6.1	4.3	26.4
Specimen 5	114.5	35	6.1	4.2	25.8
Specimen 6	114.5	36	6.2	4.2	26.0
Specimen 7	114.5	35	6.2	4.2	26.0
Batch 6					
Specimen 1	114.5	35	6.2	4.2	26.2
Specimen 2	114.5	35	6.2	4.2	26.4
Specimen 3	114.5	34	6.1	4.2	25.3
Specimen 4	114.6	34	6.2	4.4	27.1
Specimen 5	114.6	32	6.2	4.3	27.0
Specimen 6	114.5	34	6.2	4.4	27.4
Specimen 7	114.5	33	6.2	4.4	27.2

Appendix B: Acetone measurements during vapour smoothing

	Mass of petri dish containing acetone (g)		
	Before smoothing	After smoothing	Mass of vaporized acetone (g)
Batch 3			
Specimen 1	45.3	36.8	8.5
Specimen 2	45.3	36.8	8.5
Specimen 3	45.3	36.8	8.5
Specimen 4	44.9	35.3	9.6
Specimen 5	44.9	35.3	9.6
Specimen 6	44.9	35.3	9.6
Specimen 7	45.2	36.4	8.8
Batch 6			
Specimen 1	41.9	36.6	5.3
Specimen 2	41.9	36.6	5.3
Specimen 3	41.9	36.6	5.3
Specimen 4	40.5	35.0	5.5
Specimen 5	40.5	35.0	5.5
Specimen 6	40.5	35.0	5.5
Specimen 7	43.1	35.7	7.4

Appendix C: Matlab code

```
%Plot surface roughness graphs of both treated and untreated specimens  
%Find Ra value
```

```
clear all  
clc
```

```
%Bring in surface roughness text files  
filename = 'Batch 6/sample 1.csv' ;  
M = csvread(filename,7,0) ;
```

```
%Bring in surface roughness text files after smoothing  
filename2 = 'Batch 6 (After smoothing)/sample 1.csv' ;  
M2 = csvread(filename2,7,0) ;
```

```
%X and Y vectors  
X = M(:,1) ;  
Y = M(:,2) ;
```

```
%X and Y vectors  
X2 = M2(:,1) ;  
Y2 = M2(:,2) ;
```

```
%Trapezoidal rule  
Q = trapz(X,abs(Y)) ;  
Ra = Q/max(X)
```

```
%Plot X vs. Y  
figure ;  
hold on ;  
grid on ;
```

```
plot(X, Y)  
plot(X2, Y2)  
xlabel('X ( $\mu\text{m}$ )')  
ylabel('Y ( $\mu\text{m}$ )')  
xlim([0 3500])  
ylim([-40 30])  
legend('Before smoothing','After smoothing','Location','southeast')
```

```
%Calculate strain using extensometer displacement values and gauge length  
%Plot stress vs. strain graphs from Zwick data
```

```
clear all  
clc
```

```
%Bring in strain text files  
filename1 = 'Batch6ResultsS1.txt' ;  
Z1 = dlmread(filename1,'t',3,0) ;
```

```
%Strain and time vectors  
displacement1 = Z1(:,2) ;  
g_length1 = input('Gauge length?');  
strain1 = displacement1/g_length1 ;
```

```
%Stress vectors  
force1 = Z1(:,3);  
stress1 = force1/(4.2*6.2) ;
```

```
%Bring in strain text files  
filename2 = 'Batch6ResultsS2.txt' ;  
Z2 = dlmread(filename2,'t',3,0) ;
```

```

%Strain and time vectors
displacement2 = Z2(:,2) ;
g_length2 = input('Gauge length?');
strain2 = displacement2/g_length2 ;

%Stress vectors
force2 = Z2(:,3);
stress2 = force2/(4.2*6.2) ;

%Bring in strain text files
filename3 = 'Batch6ResultsS3.txt' ;
Z3 = dlmread(filename3, '\t',3,0) ;

%Strain and time vectors
displacement3 = Z3(:,2) ;
g_length3 = input('Gauge length?');
strain3 = displacement3/g_length3 ;

%Stress vectors
force3 = Z3(:,3);
stress3 = force3/(4.2*6.1) ;

%Bring in strain text files
filename4 = 'Batch6ResultsS4.txt' ;
Z4 = dlmread(filename4, '\t',3,0) ;

%Strain and time vectors
displacement4 = Z4(:,2) ;
g_length4 = input('Gauge length?');
strain4 = displacement4/g_length4 ;

%Stress vectors
force4 = Z4(:,3);
stress4 = force4/(4.4*6.2) ;

%Bring in strain text files
filename5 = 'Batch6ResultsS5.txt' ;
Z5 = dlmread(filename5, '\t',3,0) ;

%Strain and time vectors
displacement5 = Z5(:,2) ;
g_length5 = input('Gauge length?');
strain5 = displacement5/g_length1 ;

%Stress vectors
force5 = Z5(:,3);
stress5 = force5/(4.3*6.2) ;

%Bring in strain text files
filename6 = 'Batch6ResultsS6.txt' ;
Z6 = dlmread(filename6, '\t',3,0) ;

%Strain and time vectors
displacement6 = Z6(:,2) ;
g_length6 = input('Gauge length?');
strain6 = displacement6/g_length6 ;

%Stress vectors
force6 = Z6(:,3);
stress6 = force6/(4.4*6.2) ;

%Bring in strain text files
filename7 = 'Batch6ResultsS7.txt' ;
Z7 = dlmread(filename7, '\t',3,0) ;

```

```

%Strain and time vectors
displacement7 = Z7(:,2) ;
g_length7 = input('Gauge length?');
strain7 = displacement7/g_length7 ;

%Stress vectors
force7 = Z7(:,3);
stress7 = force7/(4.4*6.2) ;

%Plot stress vs. strain
figure ;
hold on;
grid on;

plot(strain1, stress1)
plot(strain2, stress2)
plot(strain3, stress3)
plot(strain4, stress4)
plot(strain5, stress5)
plot(strain6, stress6)
plot(strain7, stress7)
axis([0 inf 0 inf])
xlabel('Engineering Strain (mm/mm)')
ylabel('Engineering Stress (MPa)')
legend('Specimen1','Specimen2','Specimen3','Specimen4','Specimen5','Specimen6','Specimen7','Location','southeast');

%Truncate strain values from DIC
%Plot multiple curves for each batch of stress vs strain from DIC on same axis

clear all
clc

%Bring in strain text files
filename1 = 'B6S1g.txt' ;
M1 = dlmread(filename1, '\t',3,0) ;

%Strain (mstrain) and time vectors
strain1 = M1(:,2)*0.001 ;
time_strain1 = (M1(:,1)*0.33) ;%step no. times by time frame

%Manipulate strain graphs
%Cut graphs at max strain
i1 = find(strain1 == max(strain1)) ;
strain1(i1+1:end)=[] ;
time_strain1(i1+1:end) = [] ;

%Plot strain vs. time
figure ;
hold on ;
grid on ;

plot(time_strain1, strain1)
axis([0 inf 0 inf])
xlabel('Time (s)')
ylabel('Strain')

%Find linear section of graph
Upp1 = input('Upper linear section?');
Low1 = input('Lower linear section?');
Alt_strain1 = strain1;
Alt_time_strain1 = time_strain1;
y_21 = find(Alt_strain1 < Upp1,1,'last');
Alt_strain1(y_21:end) = [] ;
Alt_time_strain1(y_21:end) = [] ;
y_11 = find(Alt_strain1 > Low1,1,'first');
Alt_strain1(1:y_11) = [] ;

```

```

Alt_time_strain1(1:y_11) = [] ;

%Polyfit values for linear section of the graph and x-int of linear graph
p1 = polyfit(Alt_time_strain1,Alt_strain1,1);
m1 = p1(1);
c1 = p1(2);
x_in1 = -c1/m1;

%Now shift strain graph
Fin_time_strain1 = time_strain1 - x_in1 ;

%Bring in force text files
filename1a = 'Batch6ResultsS1.txt' ;
Z1 = dlmread(filename1a, '\t',3,0) ;

%Force to stress and time vectors
force1 = Z1(:,3)' ;
stress1 = force1/(4.2*6.2)' ; %mm therefore MPa
time_stress1 = Z1(:,1)' ;

%Find stress values that are on strain timeline
stress_coarse1 = interp1(time_stress1, stress1, Fin_time_strain1);

%Bring in strain text files
filename2 = 'B6S2g.txt' ;
M2 = dlmread(filename2, '\t',3,0) ;

%Strain (mstrain) and time vectors
strain2 = M2(:,2)*0.001 ;
time_strain2 = (M2(:,1)*0.33)' ;%step no. times by time frame

%Manipulate strain graphs
%Cut graphs at max strain
i2 = find(strain2 == max(strain2)) ;
strain2(i2+1:end)=[] ;
time_strain2(i2+1:end) = [] ;

%Plot strain vs. time
figure ;
hold on ;
grid on ;

plot(time_strain2, strain2)
axis([0 inf 0 inf])
xlabel('Time (s)')
ylabel('Strain')

%Find linear section of graph
Upp2 = input('Upper linear section?');
Low2 = input('Lower linear section?');
Alt_strain2 = strain2;
Alt_time_strain2 = time_strain2;
y_22 = find(Alt_strain2 < Upp2,1,'last');
Alt_strain2(y_22:end) = [] ;
Alt_time_strain2(y_22:end) = [] ;
y_12 = find(Alt_strain2 > Low2,1,'first');
Alt_strain2(1:y_12) = [] ;
Alt_time_strain2(1:y_12) = [] ;

%Polyfit values for linear section of the graph and x-int of linear graph
p2 = polyfit(Alt_time_strain2,Alt_strain2,1);
m2 = p2(1);
c2 = p2(2);
x_in2 = -c2/m2;

%Now shift strain graph

```

```

Fin_time_strain2 = time_strain2 - x_in2 ;

%Bring in force text files
filename2a = 'Batch6ResultsS2.txt' ;
Z2 = dlmread(filename2a, '\t', 3, 0) ;

%Force to stress and time vectors
force2 = Z2(:, 3) ;
stress2 = force2 / (4.2 * 6.2) ; %mm therefore MPa
time_stress2 = Z2(:, 1) ;

%Find stress values that are on strain timeline
stress_coarse2 = interp1(time_stress2, stress2, Fin_time_strain2);

%Bring in strain text files
filename3 = 'B6S3g.txt' ;
M3 = dlmread(filename3, '\t', 3, 0) ;

%Strain (mstrain) and time vectors
strain3 = M3(:, 2) * 0.001 ;
time_strain3 = (M3(:, 1) * 0.33) ; %step no. times by time frame

%Manipulate strain graphs
%Cut graphs at max strain
i3 = find(strain3 == max(strain3)) ;
strain3(i3+1:end) = [] ;
time_strain3(i3+1:end) = [] ;

%Plot strain vs. time
figure ;
hold on ;
grid on ;

plot(time_strain3, strain3)
axis([0 inf 0 inf])
xlabel('Time (s)')
ylabel('Strain')

%Find linear section of graph
Upp3 = input('Upper linear section?');
Low3 = input('Lower linear section?');
Alt_strain3 = strain3;
Alt_time_strain3 = time_strain3;
y_23 = find(Alt_strain3 < Upp3, 1, 'last');
Alt_strain3(y_23:end) = [] ;
Alt_time_strain3(y_23:end) = [] ;
y_13 = find(Alt_strain3 > Low3, 1, 'first');
Alt_strain3(1:y_13) = [] ;
Alt_time_strain3(1:y_13) = [] ;

%Polyfit values for linear section of the graph and x-int of linear graph
p3 = polyfit(Alt_time_strain3, Alt_strain3, 1);
m3 = p3(1);
c3 = p3(2);
x_in3 = -c3/m3;

%Now shift strain graph
Fin_time_strain3 = time_strain3 - x_in3 ;

%Bring in force text files
filename3a = 'Batch6ResultsS3.txt' ;
Z3 = dlmread(filename3a, '\t', 3, 0) ;

%Force to stress and time vectors
force3 = Z3(:, 3) ;
stress3 = force3 / (4.2 * 6.1) ; %mm therefore MPa
time_stress3 = Z3(:, 1) ;

```

```

%Find stress values that are on strain timeline
stress_coarse3 = interp1(time_stress3, stress3, Fin_time_strain3);

%Bring in strain text files
filename4 = 'B6S4g.txt' ;
M4 = dlmread(filename4, '\t',3,0) ;

%Strain (mstrain) and time vectors
strain4 = M4(:,2)*0.001 ;
time_strain4 = (M4(:,1)*0.33) ;%step no. times by time frame

%Manipulate strain graphs
%Cut graphs at max strain
i4 = find(strain4 == max(strain4)) ;
strain4(i4+1:end)=[] ;
time_strain4(i4+1:end) = [] ;

%Plot strain vs. time
figure ;
hold on ;
grid on ;

plot(time_strain4, strain4)
axis([0 inf 0 inf])
xlabel('Time (s)')
ylabel('Strain')

%Find linear section of graph
Upp4 = input('Upper linear section?');
Low4 = input('Lower linear section?');
Alt_strain4 = strain4;
Alt_time_strain4 = time_strain4;
y_24 = find(Alt_strain4 < Upp4,1,'last');
Alt_strain4(y_24:end) = [] ;
Alt_time_strain4(y_24:end) = [] ;
y_14 = find(Alt_strain4 > Low4,1,'first');
Alt_strain4(1:y_14) = [] ;
Alt_time_strain4(1:y_14) = [] ;

%Polyfit values for linear section of the graph and x-int of linear graph
p4 = polyfit(Alt_time_strain4,Alt_strain4,1);
m4 = p4(1);
c4 = p4(2);
x_in4 = -c4/m4;

%Now shift strain graph
Fin_time_strain4 = time_strain4 - x_in4 ;

%Bring in force text files
filename4a = 'Batch6ResultsS4.txt' ;
Z4 = dlmread(filename4a, '\t',3,0) ;

%Force to stress and time vectors
force4 = Z4(:,3) ;
stress4 = force4/(4.4*6.2) ; %mm therefore MPa
time_stress4 = Z4(:,1) ;

%Find stress values that are on strain timeline
stress_coarse4 = interp1(time_stress4, stress4, Fin_time_strain4);

%Bring in strain text files
filename5 = 'B6S5g.txt' ;
M5 = dlmread(filename5, '\t',3,0) ;

```

```

%Strain (mstrain) and time vectors
strain5 = M5(:,2)*0.001 ;
time_strain5 = (M5(:,1)*0.33)' ;%step no. times by time frame

%Manipulate strain graphs
%Cut graphs at max strain
i5 = find(strain5 == max(strain5)) ;
strain5(i5+1:end)=[] ;
time_strain5(i5+1:end) = [] ;

%Plot strain vs. time
figure ;
hold on ;
grid on ;

plot(time_strain5, strain5)
axis([0 inf 0 inf])
xlabel('Time (s)')
ylabel('Strain')

%Find linear section of graph
Upp5 = input('Upper linear section?');
Low5 = input('Lower linear section?');
Alt_strain5 = strain5;
Alt_time_strain5 = time_strain5;
y_25 = find(Alt_strain5 < Upp5,1,'last');
Alt_strain5(y_25:end) = [] ;
Alt_time_strain5(y_25:end) = [] ;
y_15 = find(Alt_strain5 > Low5,1,'first');
Alt_strain5(1:y_15) = [] ;
Alt_time_strain5(1:y_15) = [] ;

%Polyfit values for linear section of the graph and x-int of linear graph
p5 = polyfit(Alt_time_strain5,Alt_strain5,1);
m5 = p5(1);
c5 = p5(2);
x_in5 = -c5/m5;

%Now shift strain graph
Fin_time_strain5 = time_strain5 - x_in5 ;

%Bring in force text files
filename5a = 'Batch6ResultsS5.txt' ;
Z5 = dlmread(filename5a, '\t',3,0) ;

%Force to stress and time vectors
force5 = Z5(:,3)' ;
stress5 = force5/(4.3*6.2)' ; %mm therefore MPa
time_stress5 = Z5(:,1)' ;

%Find stress values that are on strain timeline
stress_coarse5 = interp1(time_stress5, stress5, Fin_time_strain5);

%Bring in strain text files
filename6 = 'B6S6g.txt' ;
M6 = dlmread(filename6, '\t',3,0) ;

%Strain (mstrain) and time vectors
strain6 = M6(:,2)*0.001 ;
time_strain6 = (M6(:,1)*0.33)' ;%step no. times by time frame

%Manipulate strain graphs
%Cut graphs at max strain
i6 = find(strain6 == max(strain6)) ;
strain6(i6+1:end)=[] ;
time_strain6(i6+1:end) = [] ;

```

```

%Plot strain vs. time
figure ;
hold on ;
grid on ;

plot(time_strain6, strain6)
axis([0 inf 0 inf])
xlabel('Time (s)')
ylabel('Strain')

%Find linear section of graph
Upp6 = input('Upper linear section?');
Low6 = input('Lower linear section?');
Alt_strain6 = strain6;
Alt_time_strain6 = time_strain6;
y_26 = find(Alt_strain6 < Upp6,1,'last');
Alt_strain6(y_26:end) = [] ;
Alt_time_strain6(y_26:end) = [] ;
y_16 = find(Alt_strain6 > Low6,1,'first');
Alt_strain6(1:y_16) = [] ;
Alt_time_strain6(1:y_16) = [] ;

%Polyfit values for linear section of the graph and x-int of linear graph
p6 = polyfit(Alt_time_strain6,Alt_strain6,1);
m6 = p6(1);
c6 = p6(2);
x_in6 = -c6/m6;

%Now shift strain graph
Fin_time_strain6 = time_strain6 - x_in6 ;

%Bring in force text files
filename6a = 'Batch6ResultsS6.txt' ;
Z6 = dlmread(filename6a, '\t',3,0) ;

%Force to stress and time vectors
force6 = Z6(:,3)';
stress6 = force6/(4.4*6.2) ; %mm therefore MPa
time_stress6 = Z6(:,1)';

%Find stress values that are on strain timeline
stress_coarse6 = interp1(time_stress6, stress6, Fin_time_strain6);

%Bring in strain text files
filename7 = 'B6S7g.txt' ;
M7 = dlmread(filename7, '\t',3,0) ;

%Strain (mstrain) and time vectors
strain7 = M7(:,2)*0.001 ;
time_strain7 = (M7(:,1)*0.33)'; %step no. times by time frame

%Manipulate strain graphs
%Cut graphs at max strain
i7 = find(strain7 == max(strain7)) ;
strain7(i7+1:end)=[] ;
time_strain7(i7+1:end) = [] ;

%Plot strain vs. time
figure ;
hold on ;
grid on ;

plot(time_strain7, strain7)
axis([0 inf 0 inf])
xlabel('Time (s)')
ylabel('Strain')

```

```

%Find linear section of graph
Upp7 = input('Upper linear section?');
Low7 = input('Lower linear section?');
Alt_strain7 = strain7;
Alt_time_strain7 = time_strain7;
y_27 = find(Alt_strain7 < Upp7,1,'last');
Alt_strain7(y_27:end) = [] ;
Alt_time_strain7(y_27:end) = [] ;
y_17 = find(Alt_strain7 > Low7,1,'first');
Alt_strain7(1:y_17) = [] ;
Alt_time_strain7(1:y_17) = [] ;

%Polyfit values for linear section of the graph and x-int of linear graph
p7 = polyfit(Alt_time_strain7,Alt_strain7,1);
m7 = p7(1);
c7 = p7(2);
x_in7 = -c7/m7;

%Now shift strain graph
Fin_time_strain7 = time_strain7 - x_in7 ;

%Bring in force text files
filename7a = 'Batch6ResultsS7.txt' ;
Z7 = dlmread(filename7a, '\t',3,0) ;

%Force to stress and time vectors
force7 = Z7(:,3)' ;
stress7 = force7/(4.4*6.2)' ; %mm therefore MPa
time_stress7 = Z7(:,1)' ;

%Find stress values that are on strain timeline
stress_coarse7 = interp1(time_stress7, stress7, Fin_time_strain7);

%Now plot stress vs. strain
figure;
hold on;
grid on;

plot(strain1, stress_coarse1)
plot(strain2, stress_coarse2)
plot(strain3, stress_coarse3)
plot(strain4, stress_coarse4)
plot(strain5, stress_coarse5)
plot(strain6, stress_coarse6)
plot(strain7, stress_coarse7)
axis([0 inf 0 inf])
xlabel('Engineering Strain (mm/mm)')
ylabel('Engineering Stress (MPa)')
legend('Specimen1','Specimen2','Specimen3','Specimen4','Specimen5','Specimen6','Specimen7','Location', 'southeast');

%Plot stress vs DIC strain graph
%Find Elastic Modulus and strain at fracture
%Also maximum stress on DIC graphs

clear all
clc

%Bring in strain text files
filename = 'B1S1g.txt' ;
M = dlmread(filename, '\t',3,0) ;

%Strain (mstrain) and time vectors
strain = M(:,2)*0.001 ;
time_strain = (M(:,1)*0.33)' ; %step no. times by time frame

```

```

figure;
hold on;
grid on;
axis([0 inf 0 inf])
plot(time_strain, strain)
xlabel('Time (s)')
ylabel('Engineering Strain (mm/mm)')

%Manipulate strain graphs
%Cut graphs at max strain
i = find(strain == max(strain)) ;
strain(i+1:end)=[] ;
time_strain(i+1:end) = [] ;

%Plot strain vs. time
figure ;
hold on ;
grid on ;

plot(time_strain, strain)
axis([0 inf 0 inf])
xlabel('Time (s)')
ylabel('Strain')

%Find linear section of graph
Upp = input('Upper linear section?');
Low = input('Lower linear section?');
Alt_strain = strain;
Alt_time_strain = time_strain;
y_2 = find(Alt_strain < Upp,1,'last');
Alt_strain(y_2:end) = [] ;
Alt_time_strain(y_2:end) = [] ;
y_1 = find(Alt_strain > Low,1,'first');
Alt_strain(1:y_1) = [] ;
Alt_time_strain(1:y_1) = [] ;

%Polyfit values for linear section of the graph and x-int of linear graph
p = polyfit(Alt_time_strain,Alt_strain,1);
m = p(1);
c = p(2);
x_in = -c/m;

%Now shift strain graph
Fin_time_strain = time_strain - x_in ;

%Bring in force text files
filename1 = 'Batch1fS2.txt' ;
Z = dlmread(filename1,'\t',3,0) ;

%Force to stress and time vectors
force = Z(:,3) ;
stress = force/(4.0*6.4) ; %mm therefore MPa
time_stress = Z(:,1) ;

%Find stress values that are on strain timeline
stress_coarse = interp1(time_stress, stress, Fin_time_strain);

%Now that have same points, plot stress vs. strain
figure;
hold on;
grid on;

plot(strain, stress_coarse)
axis([0 inf 0 inf])
xlabel('Strain')
ylabel('Stress (MPa)')

```

```

%Find slope of stress strain to get Elastic Modulus
Upp1 = input('Upper linear section?');
Low1 = input('Lower linear section?');
Alt_stress = stress_coarse;
Alt_strain2 = strain;
y_4 = find(Alt_stress < Upp1,1,'last');
Alt_stress(y_4:end) = [];
Alt_strain2(y_4:end) = [];
y_3 = find(Alt_stress > Low1,1,'first');
Alt_stress(1:y_3) = [];
Alt_strain2(1:y_3) = [];

%Polyfit values for linear section of the graph and x-int of linear graph
p_ss = polyfit(Alt_strain2,Alt_stress,1) ;
m_YM = p_ss(1)
c_YM = p_ss(2) ;
x_in1 = -c_YM/m_YM ;
YM_line = m_YM*Alt_strain2+c_YM ;

p_ss2 = polyfit(Alt_strain_O,Alt_stress,1);
m_YM2 = p_ss2(1);
c_YM2 = p_ss2(2);
x_in2 = -c_YM2/m_YM2
YM_line_2 = m_YM2*Alt_strain_O+c_YM2;

%Now plot stress vs. strain with Elastic Modulus line
figure;
hold on;
grid on;

plot(strain,stress_coarse)
plot(Alt_strain2,YM_line,'r')
axis([0 inf 0 inf])
xlabel('Strain')
ylabel('Stress (MPa)')

%Strain at fracture
strain_fracture = max(strain)

%Max stress on DIC graphs
stress_max = max(stress_coarse)

```

Appendix D: Budget

Item	Amount	Unit cost (Rands)	Total cost (Rands)
Roll of ABS filament	1	450.00	450.00
Polypropylene (PP) container	1	75.00	75.00
PlexiGlas sheet	0.6m ²	1042.00 /m ²	625.40
Total			1150.40

Appendix E: Risk Assessment

Appendix F: Interim report